ORNL-3775
UC-80 – Reactor Technology
TID-4500 (37th ed.)

MARITIME REACTOR PROGRAM

ANNUAL PROGRESS REPORT

FOR PERIOD ENDING NOVEMBER 30, 1963

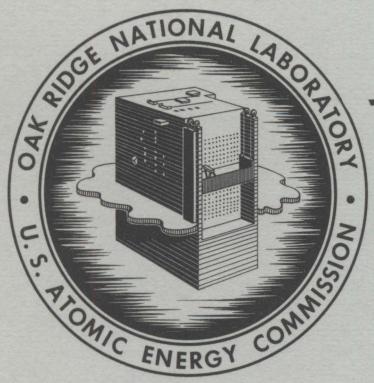

OAK RIDGE NATIONAL LABORATORY
operated by
UNION CARBIDE CORPORATION
for the
U.S. ATOMIC ENERGY COMMISSION

Printed in USA. Price $3.00. Available from the Clearinghouse for Federal Scientific and Technical Information, National Bureau of Standards, U.S. Department of Commerce, Springfield, Virginia

ORNL-3775

Contract No. W-7405-eng-26

MARITIME REACTOR PROGRAM ANNUAL PROGRESS REPORT

FOR PERIOD ENDING NOVEMBER 30, 1963

H. C. McCurdy
Program Coordinator

MARCH 1965

OAK RIDGE NATIONAL LABORATORY
Oak Ridge, Tennessee
operated by
UNION CARBIDE CORPORATION
for the
U.S. ATOMIC ENERGY COMMISSION

CONTENTS

SUMMARY

N.S. SAVANNAH Project — General Support

An experimental program, involving both laboratory studies and shipboard testing, is being conducted to determine the iodine-removal efficiency that can be expected of the activated-charcoal units installed aboard the N.S. SAVANNAH. Forty-three tests were completed on three types of charcoal under various combinations of temperature and humidity. In most of these tests the charcoal units exhibited high iodine-removal efficiency. However, abnormal penetration of iodine was observed in some tests. A series of exploratory experiments indicated that the abnormal penetration was probably caused by variations in the iodine sources. The sources were found to contain, but not necessarily at all times, two or more components: a large, less volatile fraction composed mainly of elemental iodine, and a smaller more volatile fraction that appeared to be composed of nonelemental compounds. Efforts are continuing to identify the various forms of iodine and to characterize more fully their behavior in activated-charcoal adsorbers.

Concurrently with the laboratory investigations, in-place tests on the shipboard reactor-compartment ventilation system were conducted to demonstrate that the installation of the iodine-adsorption equipment is such that the potential iodine-removal efficiency of charcoal can, in fact, be realized. During the current reporting period, four series of ^{127}I tests and two series of ^{131}I tests were made using the two types of test procedures previously developed. With one exception, all the tests indicated satisfactory iodine-removal efficiency. Results of ^{127}I tests performed in August 1963 indicated a reduction in the efficiency of the starboard unit. However, subsequent tests of the same system using both the ^{127}I and ^{131}I procedures yielded satisfactorily high efficiencies. It appears that the August test results were probably in error due to either an unobserved test malfunction, tramp iodine contamination, or faulty analytical techniques. It is concluded, with some slight reservation regarding the starboard unit, that the N.S. SAVANNAH reactor-compartment ventilation system is capable of achieving at least the iodine-removal

efficiency observed in a series of 14 laboratory tests of 11-in.-square SAVANNAH-type charcoal units under simulated accident conditions. These tests, conducted with continuous iodine injection at 96 to 100°C and with 80 to 90% saturated steam in air, showed the efficiency of the charcoal unit alone to be 99.86 ± 0.07% at the 95% confidence level.

Another type of in-place test that is routinely performed on the N.S. SAVANNAH reactor-compartment ventilation system is designed to demonstrate that the high-efficiency particulate filters are correctly installed. The testing procedure is an adaptation of the standard DOP (dioctylphthalate) technique. Until recently, these tests were performed by ORNL personnel, including two series of tests during the current report period. Assistance was then provided to the operating agent in establishing shipboard capability so that these tests could be made by the regular ship's crew. This assistance included aid in specifying and procuring the necessary test equipment and in training of the operator's personnel. States Marine Lines personnel were trained and assumed responsibility for the tests. Following the change in operating agents, personnel of the American Export & Isbrandtsen Lines were trained, and the in-place particulate-filter efficiency tests are presently performed by the ship's crew.

A study was made of the time delay in activity release afforded by the reactor compartment and the effect of this delay in reducing the dose from noble gases that could be released from the N.S. SAVANNAH as a consequence of the maximum credible accident. Generalized relations were derived for the release rate of a given isotope from the second container of a double-containment system. A graphical presentation of the release rate is given in dimensionless form. Expressions were also obtained for the dose resulting from core releases into single- and double-containment systems. The noble-gas dose reduction due to reactor-compartment holdup in the N.S. SAVANNAH was determined for three different compartment exhaust rates. The results of this analysis show that it would be desirable to reduce the reactor-compartment exhaust rate to the lowest possible value consistent with the negative pressure requirement.

A calculation was performed to determine the effect of particle agglomeration on the activity release from a containment system that depends

on particulate filtration for its effectiveness. The calculation was based on a simplified model that is shown to be conservative. Since iodine is of major concern in filtration problems, it was chosen to illustrate the particle behavior. Results of this analysis indicate that for maximum credible accident conditions in N.S. SAVANNAH containment, agglomeration occurs at a rate fast enough to prevent significant penetration of the filtration systems, even if all particles of a size smaller than 0.3 μ are assumed to penetrate the filters.

Refueling of the N.S. SAVANNAH reactor will require moving the spent fuel elements from the ship to the shore fuel-handling facility in a transfer cask that has a capacity of one fuel element. For accident analysis, it was of interest to estimate fuel cladding and cask temperatures following simultaneous loss of primary and secondary coolant from the cask. Under this condition, radiant heat transfer would be the primary mechanism for removing decay heat. A calculation was made using a computer method developed at ORNL for predicting the temperature distribution in a fuel bundle of rods in a parallel array. Depending upon the extent to which the lead shielding is bonded to the steel shell of the cask and upon the emissivity of the various components, peak cladding temperatures were estimated to reach 1220 to 1540°F if the transfer accident occurred at 10 days after reactor shutdown.

Before the N.S. SAVANNAH visits a port, a survey of the port is made to select a berth meeting N.S. SAVANNAH site requirements and to establish an emergency plan for removing the ship in case of an accident. The Laboratory continued to assist the ship's operator in making these surveys. During the current report period, survey visits were made to several coastal cities in northern Europe and the eastern United States.

A control rod positioning program previously prepared for use with N.S. SAVANNAH core I and the replacement rod drive system developed by the Marvel-Schebler Division of Borg-Warner Corporation was reviewed in light of physics measurements made during subsequent operation of the ship. These measurements had yielded data sufficiently different from the original assumptions to warrant recomputing the program. A revised program

intended as a basis for initial sequence-controller settings was prepared and submitted to the AEC-Maritime Administration Joint Group.

Advanced Core Development

Previously reported studies indicated that a significant reduction in N.S. SAVANNAH fuel-cycle cost could be obtained by increasing the core lifetime. This observation prompted further studies of cores in which boron burnable poison was added to the stainless steel fuel tubing to obtain the additional reactivity control that is necessary for longer core life. Physics calculations were made to determine the reactivity lifetimes that could be achieved with various ^{10}B loadings. The restriction was applied that each core considered should have the same shutdown reactivity margin that is provided in the original core I loading. The effect of the added ^{10}B and fuel on the worth of the control rods was considered.

The longest core life treated (~6 full-power years) was attained with a ^{10}B loading of 200 ppm in the stainless steel fuel cladding, 6 wt % ^{235}U fuel enrichment, and Zircaloy fuel containers. With a load factor of 0.67, two core loadings would serve for the usual 20-year life expectancy of a ship. Fuel-cycle cost analyses were made for the families of cores covered in the physics calculations. The results indicated decreasing fuel-cycle costs with increasing core life but little economic incentive for lifetime beyond 4.5 full-power years for cores with either stainless steel or Zircaloy fuel-element containers. The state of knowledge regarding potential metallurgical problems associated with long-lived cores was investigated, and it was concluded that high-burnup tests on prototype fuel elements would be useful in assessing their stability for 4.5 full-power years.

Estimates were made of the linear power outputs at which fuel-melting would occur in six water-cooled power reactors, which were selected to give a representative cross section of current reactors of the water-cooled, bulk-UO_2-fueled, low-enrichment type. The estimates were based on fuel-to-cladding thermal conductance and thermal-conductivity-integral data obtained by analysis of Canadian data for a group of 55 specimens irradiated in a hydraulic-rabbit facility and on the out-of-pile thermal

conductivity measurements of Deem and Lucks. It was found that the fuel-rod linear power outputs required for fuel melting do not vary much from reactor to reactor and, in general, range from 23 to 27 kw/ft. The N.S. SAVANNAH initial core was found to be one of the more conservative designs with respect to the reactor power level that would be required to cause fuel melting.

Fuel irradiation tests were conducted in the ORR pressurized-water loop as part of an investigation for determining the suitability of non-pelletized UO_2 fuel for use in a replacement core for the N.S. SAVANNAH. Before this work was terminated in 1962, a total of 27 fuel rods fabricated by either swaging or vibratory compaction methods were irradiated at linear heat rates up to 15 kw/ft and to burnups as high as 8250 Mwd/MT of the uranium. The results of postirradiation examination of most of these specimens were reported previously. Examination of the balance was completed during the current report period. Results are reported for visual examination, gamma scans, dimensional measurements, analyses of crud adhering to the specimens, burnup analyses, fission-gas release, metallographic studies, and determination of plutonium content.

Visual examination showed no effects of irradiation except for the presence of dark, loosely adhering oxide deposits on the surface of the rods, the deposits being generally heavier toward the ends of the rods than near the center. Gamma scans were similar to those obtained previously, showing a slight amount of flux peaking at the ends of most rods and a peak-to-average value of about 1.15. Dimensional examination showed a maximum bow of about 0.050 in. and a maximum increase in rod diameter of 7.7 mils. Analyses of the loosely adhering oxide indicated that the concentration on the surface of the rod was as much as 7.6 mg/cm^2 and that the predominant constituent was iron oxide. Burnup analyses indicated migration of ^{137}Cs in fuel rods having central voids. Release of ^{85}Kr was found to be as much as 77% of the amount formed. Metallographic examination showed changes in the structure of the UO_2 but no evidence of potential cladding failure in any of the specimens. The ^{239}Pu content was found to reach peak concentrations of between 0.48 and 1.36 mg of ^{239}Pu per g of uranium.

MARITIME REACTOR PROGRAM ANNUAL PROGRESS REPORT

1. INTRODUCTION

The purpose of the ORNL Maritime Reactor Program is to provide technical assistance to the Atomic Energy Commission–Maritime Administration Joint Group, which is responsible for directing this country's efforts to develop nuclear-powered merchant ships. This assistance program was initiated in September 1957 and has been associated primarily with the N.S. SAVANNAH project. The nature and extent of assistance activities gradually changed as the project progressed through design, construction, test, and operation stages.

Following an extended period of dockside and sea tests, the Atomic Energy Commission on August 2, 1962 authorized States Marine Lines, Inc. to operate the N.S. SAVANNAH for a period of interim sea and port operations, including the first group of port visits. This initial period of operation extended through the balance of 1962 and into the early part of 1963. During this period 11 ports were visited: Savannah, Georgia (August 22–28, 1962); Norfolk, Virginia (August 30 to September 13, 1962); east-west traverse of the Panama Canal (September 18, 1962); Seattle, Washington (October 1 to November 16, 1962); San Francisco, California (November 17–26, 1962); Long Beach, California (November 27 to December 11, 1962); Los Angeles, California (December 11–16, 1962); Honolulu, Hawaii (December 23–27, 1962); Portland, Oregon (January 4–10, 1963); San Diego, California (January 14–22, 1963); Balboa, Panama (January 29–31, 1963); west-east traverse of the Panama Canal (February 1, 1963); and Galveston, Texas (February 5, 1963). The ship entered the Todd Shipyard at Galveston on February 5, 1963 for an extended reactor and ship outage for evaluating the condition and performance of the ship and power plant and for incorporating a number of planned modifications. Up to this time the SAVANNAH had travelled 29,649 nautical miles; the reactor had generated 4315 Mwd of power (approximately 11% of the expected core life); and the ship had received a total of 339,916 visitors in the 11 ports.

Tests and modifications during the Galveston outage in early 1963 included the annual Coast Guard and ABS inspections, 1500-hr physics tests, construction of additional crew quarters, replacement of the radiation-monitoring system, extensive modifications of the reactor compartment ventilation system, and numerous minor repairs and modifications. After this work was completed, sea trials were conducted May 1–3, 1963. It was planned that the ship would visit the port of Houston, Texas on May 7, 1963, and this visit was to be followed by visits to a number of other large U.S. ports and a series of shuttle runs between east coast U.S. ports and northern European ports. However, a labor dispute prevented the scheduled departure from Galveston on May 7, 1963. This situation was the culmination of a series of labor difficulties that had troubled the project. The Department of Commerce intervened, instructed the operating agent to terminate the services of the crew, and then cancelled the contract of the operating agent.

The AEC-MARAD Joint Group immediately engaged The Babcock & Wilcox Company to take responsibility for care of the nuclear propulsion plant, operation of the reactor at dockside, and training of personnel. These functions are performed by the SAVANNAH Technical Staff, which is composed of personnel from The Babcock & Wilcox Company and Todd Shipyards Corporation. In June 1963 a group of 18 project-associated personnel began an accelerated reactor operator training course provided by Babcock & Wilcox in Galveston. The objective of the training was to provide an interim crew with enough licensed reactor operators to return the plant to operating condition by the end of 1963 and to assist in training the permanent operating crew. In July 1963, American Export & Isbrandtsen Lines of New York was selected as the new General Agent for operation of the SAVANNAH. In September, AEL personnel entered an N.S. SAVANNAH training program at the United States Merchant Marine Academy at Kings Point, New York. It is planned that these trainees will move to Galveston in December 1963 for additional training and that AEL will take custody of the ship early in 1964. The tentative schedule calls for the N.S. SAVANNAH to resume port visits in May 1964 and to follow essentially the same visit schedule as had been planned for 1963.

During the current report period, ORNL assistance to the Maritime Reactors Program included shipboard testing of iodine and particulate filters, iodine adsorption studies to further validate and to improve in-place testing procedures, reviews of proposed modifications to the reactor compartment ventilation system, assignment of a trainee to the interim crew training program, assistance in port surveys, and studies of certain aspects of reactor safety and advanced core development.

2. N.S. SAVANNAH PROJECT — GENERAL SUPPORT

Iodine-Adsorption Studies

W. E. Browning, Jr. R. E. Adams

The ventilation gases from the reactor compartment of the N.S. SAVANNAH are processed through particulate filters and iodine-sorption units to provide for control of any radioactive iodine vapor and particulate material that might be present in the compartment atmosphere as the result of an accident. Originally, two systems were provided for ventilating the compartment. The normal ventilation system was of 4000-cfm capacity, with provisions for processing the gases through three cleaning stages: (1) a prefilter, (2) a high-efficiency filter for particulate control, and (3) a silvered-copper-mesh unit for iodine control. In addition, an emergency system of 200-cfm capacity was provided that had five stages of gas cleaning: (1) a prefilter, (2) a high-efficiency filter, (3) a silvered-copper-mesh unit, (4) an activated-charcoal unit, and (5) a second silvered-copper-mesh unit. The emergency system served as a backup to the normal system and did not operate continuously. The normal system discharged to the atmosphere through the off-gas stack on the forward mast, and the emergency system discharged through two vents atop the superstructure of the ship.

The availability of two ventilation systems presented some problems. In the event of fission-product release, it would have been necessary that the main system flow be stopped and the emergency system started manually. This and the superior efficiency observed in tests of the emergency system prompted the design and installation of an improved ventilation system for the reactor compartment. The main and emergency systems were removed, and an enlarged version of the old emergency ventilation unit was installed during March–April 1963. Two parallel ventilation units are now provided, with one unit to be operated continuously at a system flow of 1000 to 1100 cfm and the other unit to be held in standby in the event of need. A continuing experimental program, involving both laboratory studies and shipboard testing, is being conducted for determining

the iodine-removal efficiency that can be expected of these units under various conditions.

Laboratory Studies

Small-scale tests are being conducted on samples of various types of charcoal to obtain semiquantitative information on their ability to adsorb iodine at design and off-design conditions. The simple experimental system initially used is pictured in Fig. 2.1. Incoming air was passed through the small, glass, steam generator and then routed into the test system from the right in the photograph. Iodine vapor (^{131}I + ^{127}I) was slowly released from the glass U-tube (maintained at the temperature of solid CO_2) to a small flow of air, which was then mixed with the main stream. The gas mixture of air, iodine vapor, and steam was

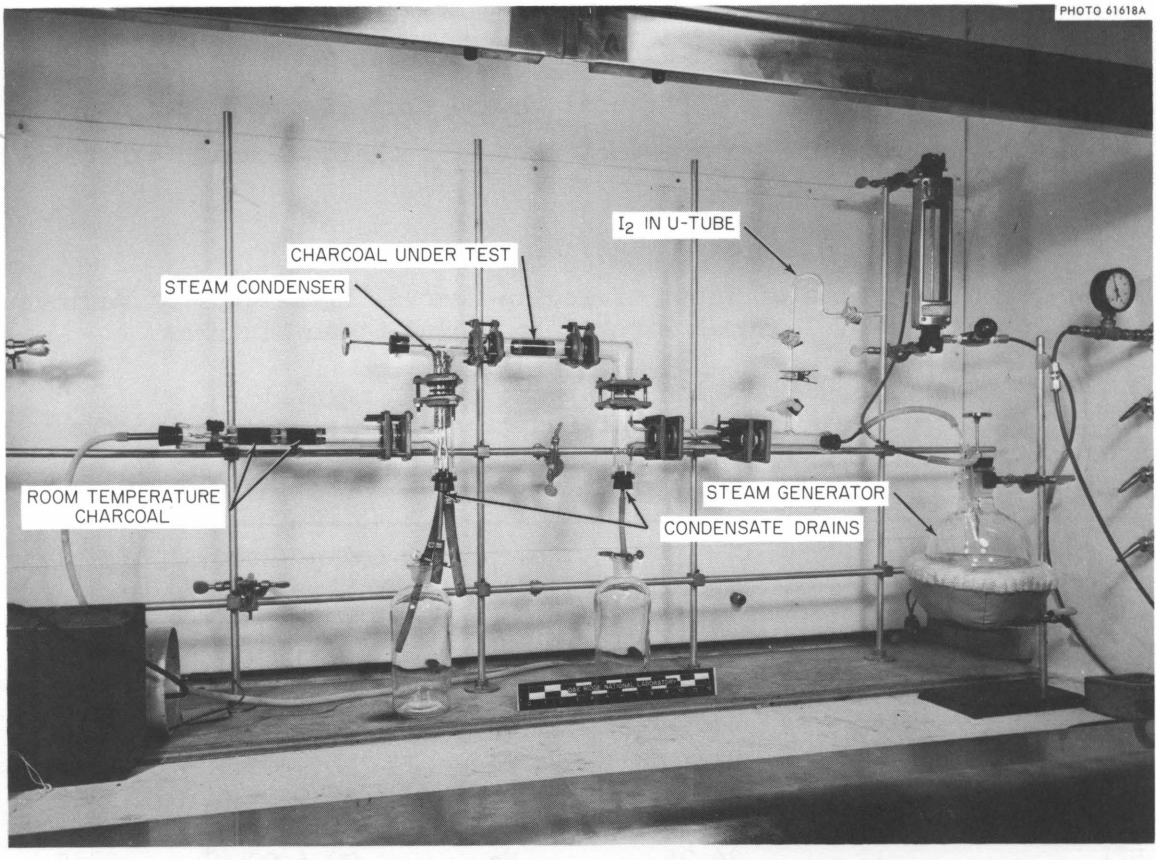

Fig. 2.1. Laboratory Equipment for Tests of Iodine Removal Efficiency of Various Types of Charcoal Exposed to an Iodine-Steam Mixture.

then passed through the charcoal unit under test. The test system was heated and insulated to a point just downstream of the charcoal unit to prevent excessive condensation of steam by the walls. After emerging from the test unit, the gas mixture was passed through silvered copper mesh wrapped around a water-cooled steam condenser and finally through two room-temperature charcoal units. Two drains were provided for steam condensate collection before and after the test unit. At the conclusion of an experiment the test system was cooled and then disassembled up to the flanged joint immediately upstream of the charcoal unit under test. The various parts and the condensates were analyzed for their ^{131}I content. With these data an iodine-adsorption efficiency for the charcoal unit could be calculated.

Forty-three tests were completed on three types of charcoal under various combinations of temperature and humidity. A summary of the results is presented in Table 2.1. The iodine-vapor concentration was estimated to be approximately 10^{-4} mg/m^3 of sweep gas; the superficial linear velocity through the charcoal ranged from 21 to 33 fpm; and the bed depth was 1.2 in. For the most part, the charcoal units exhibited

Table 2.1. Results of Tests of Iodine-Removal Efficiency of Various Types of Charcoal Exposed to Iodine-Steam Mixtures

Iodine-vapor concentration in steam: $\sim 10^{-4}$ mg/m^3
Superficial linear velocity of iodine-steam mixture: 21–33 fpm
Charcoal bed depth: 1.2 in.

Charcoal	Number of Tests	Temperature (°C)	Steam Present	Iodine-Removal Efficiency (%)	
				Range	Average
BPL	16	97–100	Yes	19.9–99.7	80.0
PCB	8	97–100	Yes	50.7–99.9	86.8
Whetlerite[a]	3	98–99	Yes	82.9–97.6	92.2
BPL	4	97–100	No	96.3–99.7	98.4
BPL	12	24–25	No	90.4–99.9+	98.5

[a]Whetlerite is BPL charcoal containing salts of silver, copper, and chromium.

what may be termed normal penetration of iodine under the conditions specified for the tests. However, abnormal penetration of iodine was observed in too many instances to be ignored. Variations in (1) the environmental conditions of the laboratory, (2) operating procedures of similar experiments, (3) materials used in construction of the experimental system, and (4) the iodine vapor sources may, either singly or in combination, have been responsible for this abnormal behavior. These and other possible causes of this rather unpredictable behavior of iodine are being subjected to continuing investigation.

A number of exploratory experiments were performed that yielded information which led to the strong suspicion that the variations listed as 1, 2, and 3 above were not the prime causes of the observed abnormal iodine penetration. However, these causes cannot be dismissed entirely. Very small particles, which appeared to be compounds of copper, were found in the compressed air supply, but no effect on iodine penetration was noted when the air supply was passed through high-efficiency membrane filters. This observation was further substantiated when bottled "breathing air," which contained no observable particles, was used in place of the compressed air. No effect was noted of varying the materials of construction in the experimental apparatus. It was found in the experiments with 100°C steam that if a special effort was made to saturate the charcoal grains with water, the iodine penetration became large. This, however, was considered to be a special laboratory condition and not likely to have occurred in all the prior experiments in which excessive penetration occurred. Saturation of the charcoal grains with water might be classed as a secondary cause but not the primary one. The net result of these exploratory experiments was the isolation of the iodine source as the probable primary cause of abnormal iodine behavior.

All the experiments discussed above were carried out with the charcoal bed under test having a nominal 1.2-in. depth of 12/30 mesh charcoal. In an effort to derive additional information concerning the nature of the iodine source, the bed depth was increased to 8 in. Experiments with the deeper bed at room temperature exhibited increased iodine-adsorption efficiency, as was expected; however, the distribution of iodine within

the charcoal mass was suggestive of elemental iodine vapor plus one or two more penetrating forms of iodine. The major fraction of the ^{131}I activity was stopped in the first 0.75 to 1.0 in. of charcoal. A small amount of ^{131}I activity was also found distributed throughout the remainder of the charcoal mass. A downstream high-efficiency filter and a secondary 8-in.-deep charcoal unit also contained small amounts of ^{131}I activity.

On the basis of these observations, an experimental system was designed that permits continuous observation of the iodine efficiency of the charcoal unit during an experiment. This system is diagrammed in Fig. 2.2 and pictured in Fig. 2.3. In tests with this system, small up- and downstream analytical sampling units were monitored by 3 × 3-in. NaI crystals coupled to a multiple-input gamma spectrometer. The rate of increase of ^{131}I activity in the upstream sampler was related to the rate

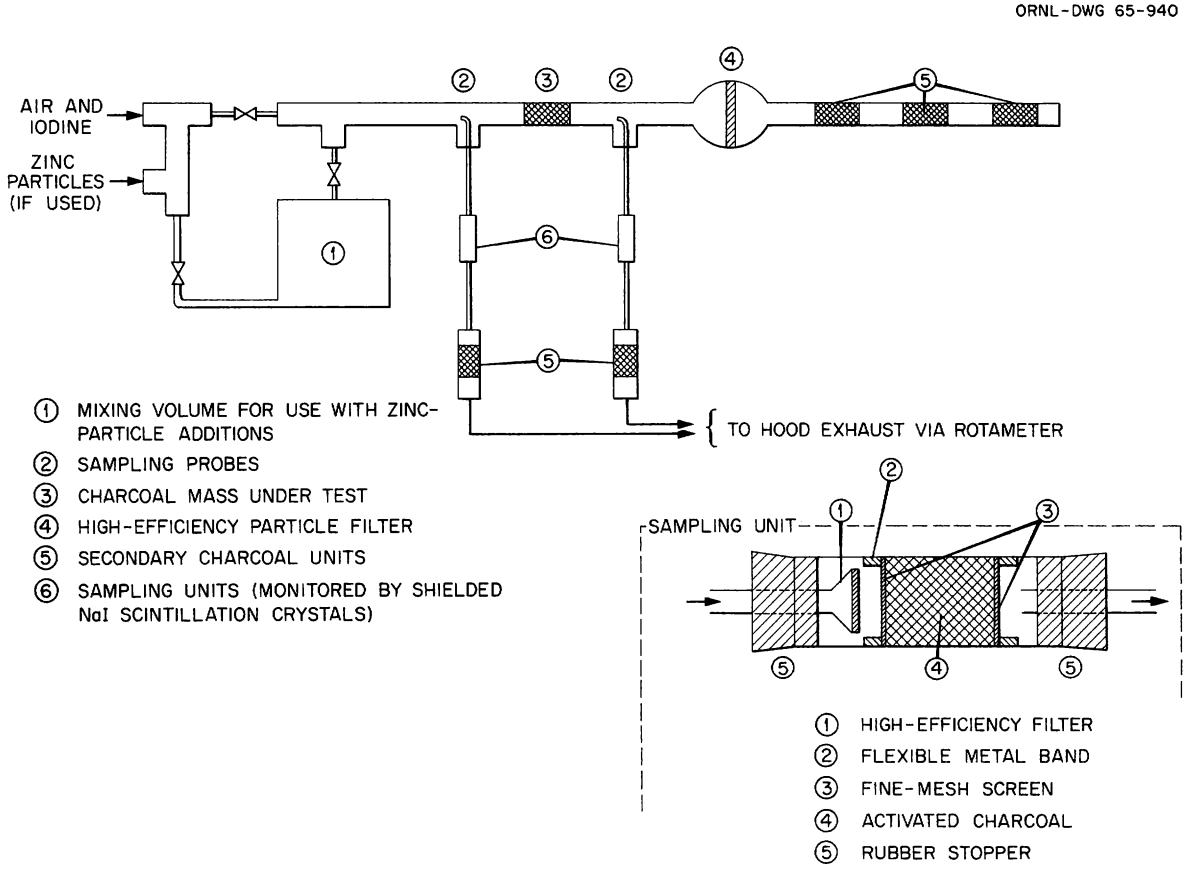

Fig. 2.2. Schematic Diagram of Laboratory Assembly for Continuous Observation of Iodine Removal Efficiency of Charcoal.

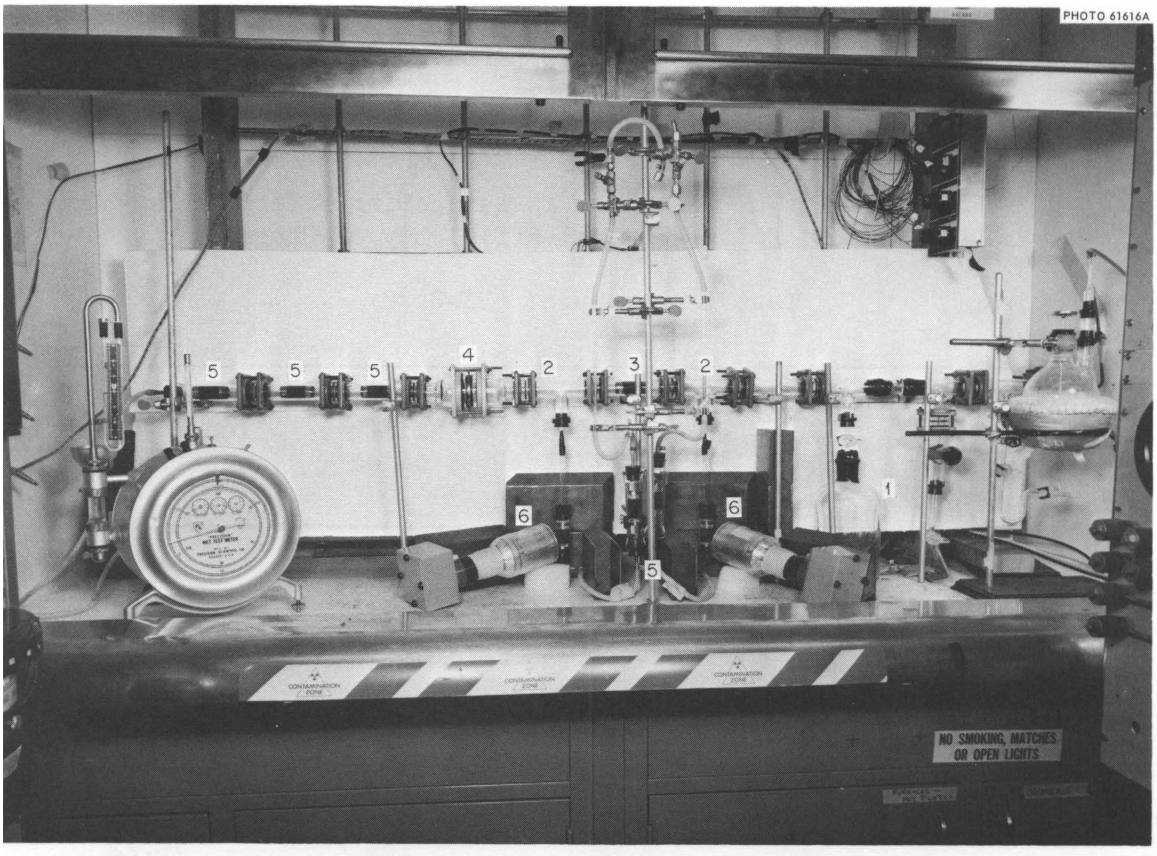

Fig. 2.3. Photograph of Laboratory Assembly for Continuous Observation of Iodine Removal Efficiency of Charcoal. See Fig. 2.2 for key to numbered units.

of transport from the iodine source, which was thermostated to the temperature produced by a freezing mixture of solid CO_2 and trichloroethylene. At the end of the experiment the main system and samplers were disassembled and analyzed for ^{131}I content. This refined apparatus was used to investigate the behavior of iodine as a function of time under several conditions that were suspected as having something to do with the variations in iodine-removal efficiency.

The effect of foreign particles in an iodine-collection system was studied briefly using zinc particles generated by passing a spark between zinc electrodes. Both nonradioactive and radioactive zinc electrodes were used in the experiments. The particle size was estimated to range between 20 and 300 A based on prior experience with this type of particle

generator.[1] The results, which were somewhat inconclusive, are listed in Table 2.2. They indicate that the particular particles used do not interfere with the iodine-removal efficiency of a charcoal unit.

Table 2.2. Results of Tests for Investigating Effect of Foreign Particles on Iodine-Removal Efficiency of Charcoal[a]

Test Temperature: 23–25°C

Air Supply	Duration of Test (hr)	Added Particles	Moisture Added	Overall Iodine-Removal Efficiency (%)
Filtered	18	None	No	99.91
	14	None	No	99.81
	17.5	None	No	99.92
	11.3	Zn fume	No	99.93
	13.6	Zn fume	No	99.77
	12.5	^{65}Zn fume	No	99.91
	12	^{65}Zn fume	No	99.93
Not filtered	12	None	No	99.98
	12	None	Yes	76.22
	18.5	None	Yes	91.88

[a]Pittsburgh BPL 12/30-mesh charcoal 1.25 in. deep used in test unit.

It was observed in some experiments that a rapid initial transport of ^{131}I activity from the source was followed by a slower, reasonably constant rate of transport. This and other observations indicate that the iodine sources contain two or more components, but not necessarily at all times. The initial, rapid release of ^{131}I activity from a source at a temperature around −70°C is suggestive of an iodine compound more volatile than elemental iodine. The gradual release of ^{131}I activity after this initial release may be characteristic of either elemental

[1]W. E. Browning, Jr., and M. D. Silverman, Measurement of Characteristic of Radioactive Aerosols Using Fibrous Filters, Nuclear Safety Program Semiann. Progr. Rept. Dec. 31, 1962, USAEC Report ORNL-3401, pp. 50–55, Oak Ridge National Laboratory.

iodine or a compound slightly more volatile than elemental iodine. Calculations made with an estimated iodine vapor pressure of 10^{-6} mm indicate that sufficient elemental iodine vapor could be transported from the source into the system to account for the ^{131}I radioactivity. However, observations of the behavior of this radioactivity in the charcoal leads to the suspicion that the less volatile fraction may be composed of elemental iodine mixed with small amounts of an iodine compound.

In an attempt to identify the components of the iodine sources, the analytical technique of mass spectrometry was applied. The residue of an iodine source that had been used in the laboratory was found to contain two rather high-molecular-weight compounds, with neither corresponding to the mass of I_2. A freshly prepared iodine source that was not allowed to reach a temperature greater than that of solid CO_2 was found to contain masses corresponding to those of HI, ICl, and I_2. Recent reports of an investigation being conducted in England indicate the presence of CH_3I in some or possibly all iodine sources.[2]

Diffusion channel analysis[3] was also used to investigate the two fractions of iodine activity. These measurements showed that the more volatile fraction deposited on a charcoal-lined diffusion tube with a diffusion coefficient of 0.1 cm^2/sec but not on silver or rubber, while the less volatile fraction primarily deposited on silver with a diffusion coefficient of 0.08 cm^2/sec, which is characteristic of molecular iodine. The less volatile fraction also contained other compounds of iodine.

In earlier experiments in which the two fractions of iodine were not distinguished, it was noted that adding moisture to the air sweep gas sometimes decreased significantly the iodine-removal efficiency of the charcoal unit and that the distribution of ^{131}I in the components downstream of the charcoal unit became abnormal compared with the distribution

---

[2]D. H. F. Atkins and A. E. J. Eggleton, Iodine Compounds Formed on Release of Carrier-Free Iodine-131, British Report AERE-M-1211, May 1963.

[3]W. E. Browning, Jr., and R. D. Ackley, Characterization of Radioactive Iodine Compounds by Diffusional Deposition, Nuclear Safety Program Semiann. Progr. Rept. June 30, 1963, USAEC Report ORNL-3483, pp. 26-28, Oak Ridge National Laboratory.

when the air sweep was dry. In the "dry" experiments, the relative humidity was approximately 1 to 3%. In the "moist" experiments the humidity was increased to approximately 60% by passing the incoming air over water. The results of these experiments are also presented in Table 2.2. In experiments where the two iodine fractions were distinguished, it was noted that moisture affected the behavior of the more volatile fraction of the iodine source to a much larger extent that it did the less volatile fraction.

Efforts to identify the various forms of iodine and to characterize fully their behavior in activated-charcoal adsorbers are continuing. It is necessary to know their identity and the circumstances of their occurrence so that an evaluation can be made of the possibility of their appearing in a reactor accident. Their behavior in adsorbers under N.S. SAVANNAH conditions needs to be investigated so that the required adsorber efficiencies may be determined. However, it should be noted that the nonelemental compounds are by no means the major fraction of the iodine vapor source. Calculations indicate that they may account for only 5% of the iodine in the source. Thus, only moderate efficiencies for removal of these forms of iodine may be required to yield adequate overall iodine-removal efficiencies.

Shipboard Tests

Concurrently with the laboratory work, a program is being conducted for developing and applying test procedures and equipment for in-place tests on the shipboard reactor-compartment ventilation system. The purpose of these tests is to demonstrate that the installation of the iodine-sorption units is such that the potential iodine-removal efficiency of the charcoal can be realized. One of the operating requirements[4] of the N.S. SAVANNAH is that an in-place test be performed at least quarterly and that the iodine-removal efficiency be at least 99.90%.

---

[4]N.S. SAVANNAH Technical Specifications, Todd/SML, Report NSS-15, p. 31, May 1963.

Tests on the original ventilation system were reported in the previous report of this series.[5] Only tests on the new ventilation system are reported here. This ventilation system includes two, parallel, activated-charcoal units, one of which is in constant operation while the other is on standby. For identification these charcoal units are designated F-1 (starboard unit) and F-2 (port unit). The F-1 unit has been in more or less constant usage since installation, and the F-2 unit has been operated for only very short periods of time.

Radioactive iodine tests are conducted by injecting elemental iodine vapor labeled with ^{131}I into the ventilation system duct at the "D" deck level and removing samples of the air stream in the duct before the charcoal unit at the "C" deck level and after the charcoal unit at the "B" deck fan room. After a 2-hr test period, the samplers are recovered and analyzed for their ^{131}I content by gamma scintillation spectrometry using the RCL-128 spectrometer aboard ship. Comparison of the ^{131}I content in the two samplers yields an iodine-removal efficiency for the charcoal unit. Figure 2.4 depicts the test system presently used.

Nonradioactive iodine tests are conducted in much the same manner as the radioactive iodine tests, with the main differences being that from 1 to 3 g of elemental iodine vapor (^{127}I) is injected into the duct and the iodine content of the sampler is determined by neutron-activation techniques. The nonradioactive iodine tests are slightly less sensitive than the radioactive iodine tests. Activated charcoal normally contains a small amount of iodine as an impurity, and in most cases the downstream samplers from an iodine test have been found to contain iodine in amounts comparable to the impurity level. To ensure that the charcoal units are not overrated in their iodine-removal efficiency, it is assumed that all the iodine found in the downstream samplers actually came from iodine penetration of the unit under test and was not originally present in the sampler as an impurity. In effect, the iodine-removal efficiencies quoted

---

[5]R. E. Adams and W. E. Browning, Jr., Iodine Adsorption Studies, pp. 10–18, Maritime Reactor Program Ann. Prog. Rept. Nov. 30, 1962, USAEC Report ORNL-3416, Oak Ridge National Laboratory.

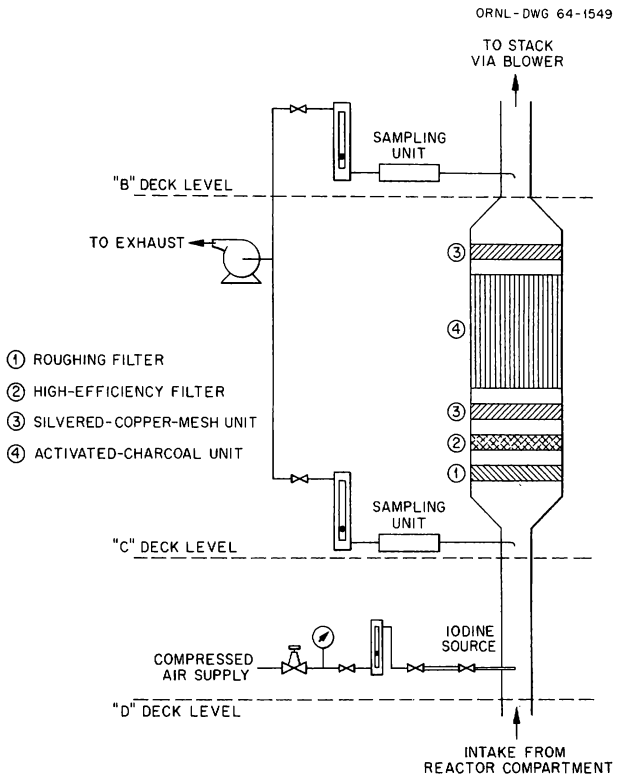

Fig. 2.4. Schematic Diagram of System for Shipboard Tests of Iodine Adsorbers.

from the nonradioactive tests represent the lower limit, and the real efficiency is in excess of the value listed.

Both ventilation systems were tested in April 1963 using radioactive and nonradioactive iodine, and the iodine-removal efficiency of each charcoal unit was satisfactory. In August 1963 both units were again tested using only nonradioactive iodine. The F-2 unit appeared satisfactory, while the F-1 unit gave an iodine-removal efficiency of about 90% in duplicate tests. A review of the test procedure and analytical determinations failed to produce sufficient information to permit the reduced efficiency of the F-1 unit to be explained by either faulty test procedures or faulty analytical techniques. A retest of the two units was conducted in September 1963, and while the F-1 unit exhibited a satisfactory iodine-removal efficiency in one of the duplicate tests, the upstream sampler contained less iodine than expected in the other test (test 9, Table 2.3). It was therefore decided to conduct another series of tests in October 1963

Table 2.3. Results of Tests of N.S. SAVANNAH Ventilation Systems with Nonradioactive Iodine

Test duration: 2 hr
System flow rate: 1050-1100 cfm

System	Date	Amount of I_2 Injected (g)	Amount of I_2 Collected (μg)		System Iodine-Removal Efficiency (%)
			Upstream	Downstream	
F-1	4-16-63	0	8.66	3.83	
		1.5	1,840.3	0.95	99.9+
		1.2	1,460.2	4.60	99.7+
	8-12-63	0	1.09	0.95	
		1.3	1,550.5	168.1	89.2
		1.6	2,381.8	202.9	91.5
	9-4-63	0	1.32	3.88	
		1.2	1,250.8	0.86	99.9+
		2.8	356.5	0.99	99.7+
	10-9-63	0	2.62	5.99	
		2.7	3,000.2	2.44	99.9+
		3.0	2,990.2	3.33	99.9+
	(a)	7.0	11,201.0	4.76	99.9+
F-2	4-16-63	0	1.42	5.33	
		1.3	1,472.9	1.07	99.9+
		1.8	1,820.5	1.33	99.9+
	8-13-63	0	9.18	49.7	
		1.1	1,271.1	5.31	99.6+
		1.3	1,574.0	6.54	99.6+
	9-5-63	0	1.53	0.80	
		2.0	2,331.8	1.29	99.9+
		1.8	2,378.9	2.94	99.9+
	10-10-63	0	2.58	1.72	
		2.7	3,470.5	2.50	99.9+
		2.5	2,650.1	3.44	99.9+

[a]Special test of 30 min duration.

using both radioactive and nonradioactive iodine in another effort to clarify the situation. In this series of tests, both charcoal systems exhibited high iodine-removal efficiencies in both types of tests. The results of the last series of nonradioactive tests, together with the results of the previous tests on these systems, are listed in Table 2.3. The results of the radioactive tests are given in Table 2.4.

Table 2.4. Results of Tests of N.S. SAVANNAH Ventilation Systems with Radioactive Iodine

Test duration: 2 hr
System flow rate: 1050–1100 cfm

System	Date	Amount of Iodine Injected		System Iodine-Removal Efficiency (%)
		^{131}I (mc)	^{127}I (mg)	
F-1	4-17-63	5	10	99.99+
		15	10	99.99+
F-2	4-18-63	5	10	99.96+
		15	10	99.99+
F-1	10-9-63	5	10	99.97+
		15	10	99.93+
F-2	10-10-63	5	10	99.96+
		15	10	99.96+

Based on the data now available, it appears that the low efficiency observed in the August tests of the F-1 system was the result of either an unobserved test malfunction, tramp iodine contamination, or faulty analytical techniques. However, two observations during the September tests tend to limit the confidence in this conclusion and support the possibility that a temporary reduction in the efficiency of the F-1 system may have actually occurred. A review of the reactor-watch log books revealed that the overall pressure drop for the F-1 system had, for no apparent reason, decreased the day after the August tests and had remained low for several weeks before returning to the value noted before the August tests. The air flow rate through the system was unchanged during this period. This reduction in pressure drop could be explained either by damage to the charcoal unit or by improper valving in routing the air through the ventilation system. The reasons for the system regaining the original pressure drop are not so obvious. The second observation was the appearance of a foreign material in the ventilation gases during the

September tests. This, as yet unidentified, material was found in significant quantities in the filter paper contained in the upstream iodine samplers from all the tests, with the exception of the background test on the F-1 system. To reach the filter paper, this material, which colored the filter paper brown, passed through the activated charcoal section of the sampler. This behavior suggests particulate rather than gaseous material. Subsequent attempts to obtain samples of this material were unsuccessful, and no evidence of this material was found during the October tests.

It is concluded, with some slight reservation, that the F-1 charcoal unit possesses sufficient iodine-removal efficiency. No doubt exists concerning the iodine-removal efficiency of the F-2 charcoal unit. Overall results from these tests during 1963 indicate that the reactor-compartment ventilation system is capable of achieving at least the iodine-removal efficiency observed in the series of 14 laboratory tests of 11-in.-square SAVANNAH-type charcoal units under simulated accident conditions.[5] These laboratory tests, which were conducted with continuous iodine injection at 96 to 100°C and with 80 to 90% saturated steam in air, showed the efficiency of the charcoal unit alone to be 99.86 ± 0.07% at the 95% confidence level.

Particulate-Filter Testing

E. C. Parrish R. W. Schneider

As indicated in the preceding section the reactor-compartment ventilation system contains high-efficiency particulate filters for removing the radioactive particles that might otherwise escape from the containment vessel in an accident situation. The operating authorization for the N.S. SAVANNAH requires that these filters be tested in place at least quarterly and that the efficiency for removal of 0.3-μ particles be at least 99.90%.[4] The testing procedure used is an adaptation of the standard DOP (dioctylphthalate) technique in which DOP smoke of known particle size is introduced into the airstream ahead of the filter, and the smoke concentration both before and after the filter is measured by means of optical instrumentation.

During the sea trials and initial port visits of the SAVANNAH in 1962 and early 1963, all in-place tests of particulate filters were performed by ORNL personnel. This arrangement required the transport of both personnel and equipment to wherever the SAVANNAH was located and involved scheduling and coordination problems that were generally a nuisance to all concerned. Therefore, an effort was made to establish procedures whereby these tests could be made by the ship's crew.

When the reactor-compartment ventilation system was modified during the Galveston outage in early 1963, provisions were made to facilitate the introduction of DOP smoke and sampling of the airstream. ORNL advised on the design of these features, assisted the operating agent (States Marine Lines, Inc.) in specifying and procuring the test equipment, furnished the DOP smoke generators, and trained States Marine personnel in the testing techniques. By the time the SAVANNAH was scheduled to leave Galveston in May 1963, the ship's crew was able to conduct the in-place DOP tests whenever required. However, because of labor difficulties and the change in operating agents which occurred at this time, the trained personnel were lost to the project. In the fall of 1963 the Laboratory therefore provided training for other personnel who were employees of the new operating agent (American Export & Isbrandtsen Lines, Inc.), with the result that the ship's crew is once again capable of conducting the in-place particulate-filter efficiency tests.

Results of two series of tests made by ORNL personnel during the current reporting period are given in Table 2.5.

Table 2.5. Results of Tests of Efficiencies of Reactor-Compartment Ventilation Systems for Removal of Particles

Date	Measured Efficiency (%)	
	System F-1 (Starboard)	System F-2 (Port)
4-10-63	99.992	99.989
8-9-63	99.998	99.996

Safety Evaluations

Holdup Effect of Double Containment (T. D. Anderson)

The N.S. SAVANNAH reactor system is enclosed in a conventional containment vessel that is, in turn, enclosed in the reactor compartment. The reactor compartment is maintained at slightly subatmospheric pressure by blowers that exhaust the compartment air through an air-cleaning system consisting of particulate filters and activated-charcoal adsorbers. In the event of an accident, controlled activity release through this air-cleaning system would result in a significant reduction in the release of the activity the air-cleaning system is designed to remove. A schematic diagram of the containment system is presented in Fig. 2.5.

The original purpose of the reactor-compartment and its ventilation system was to reduce the release to the atmosphere of particulate fission products and radioiodine in the event of an accident. An additional effect of the reactor compartment, which is the one of present interest, is the possible time delay in activity release it can provide. This time delay would result in a short-term reduction in the dose from all airborne radioactive materials; and, if decay of the isotope causing the dose were sufficiently rapid, a permanent reduction in dose would result.

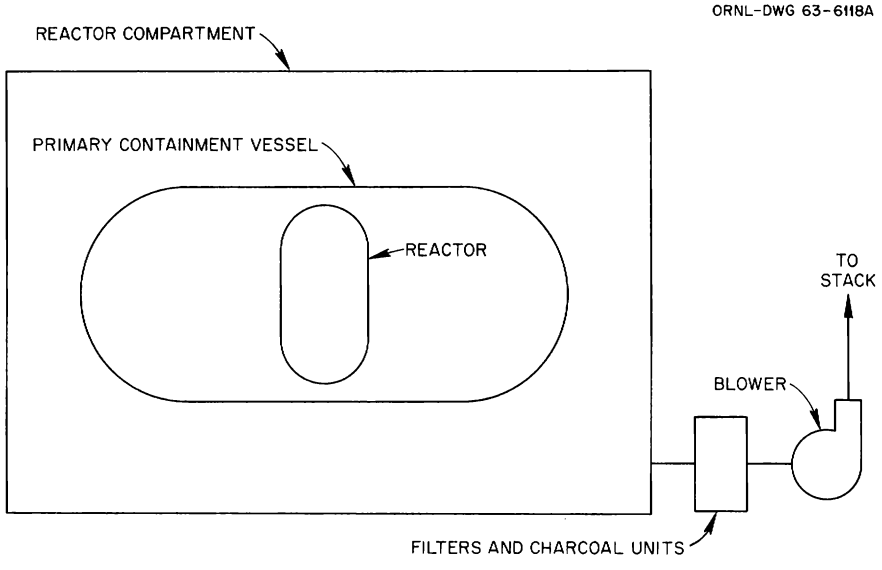

Fig. 2.5. Schematic Diagram of N.S. SAVANNAH Containment System.

Even a temporary reduction in activity release following a reactor accident could be significant, since the additional time available could be used for taking measures that would reduce the consequences of the accident. The double-containment holdup effect could be especially important for ship reactors, since it would provide time for moving the system away from populated areas shortly after the accident.

The extent to which the holdup effect would alleviate environmental hazards resulting from a reactor accident would depend on the containment system parameters, the characteristics of the isotope causing the dose, and the manner in which radioactive materials were released from the reactor. These factors have been investigated to determine the effectiveness of double-containment holdup in reducing the dose from noble gases that could be released from the N.S. SAVANNAH as a consequence of the maximum credible accident.[6]

Rate of Release from Containment System. As was shown previously,[7] the release rate, S(t), of a given isotope from the outer container of a double containment system is given by

$$S(t) = l \frac{\frac{m}{l}}{\frac{m}{l} - 1} \left[m e^{-mt} \int_0^t e^{m\tau} F(\tau)\, d\tau - l e^{-lt} \int_0^t e^{l\tau} F(\tau)\, d\tau \right] N(t) \quad , \quad (1)$$

where

$F(t)$ = fraction of the total quantity of the isotope that is outside the core at time t,

l = leak-rate constant for the inner container (fraction of the contained material that leaks out in unit time),

---

[6]T. D. Anderson, The Holdup Effect of Double-Reactor-Containment and its Influence on Dose from Airborne Radioactive Materials, paper presented at the Eighth AEC Air Cleaning Conference Held at the Oak Ridge National Laboratory, Oct. 22–25, 1963.

[7]T. D. Anderson, Time-Dependent Release of Gaseous Material from a Three-Barrier Reactor Containment System, USAEC Report ORNL TM-397, Oak Ridge National Laboratory, Nov. 16, 1962.

m = leak-rate constant for the outer container,

$N(t)$ = total quantity of the isotope in existence at time t,

t = time after the accident,

τ = variable of integration.

Equation (1) is subject to the condition that, if the isotope under consideration has precursors, these precursors move through the system in the same manner as the isotope of interest.

To evaluate the release rate given by Eq. (1), it is necessary to know the fraction of the isotope outside the core, $F(t)$. In safety analyses of power reactors it is normally assumed that some fraction, f, of the total quantity of a given fission product is released instantaneously from the core at time t_0 after the start of the accident. With this core release model, $F(t)$ is given by

$$F(t) = \begin{cases} 0 & t \leq t_0 \\ f & t > t_0 \ , \end{cases}$$

and Eq. (1) becomes

$$S(t) = \lambda f \frac{\frac{m}{\lambda}}{\frac{m}{\lambda} - 1} \left[e^{-\lambda(t-t_0)} - e^{-m(t-t_0)} \right] N(t) \ , \qquad t > t_0 \ . \tag{2}$$

As m becomes very large, Eq. (2) reduces to

$$S_1(t) = \lambda f \, e^{-\lambda(t-t_0)} \, N(t) \ , \qquad t > t_0 \ , \tag{3}$$

where $S_1(t)$ is the release rate from a single containment system.

For convenience in graphical presentation, the release rate given by Eq. (2) can be arranged in the dimensionless form

$$\frac{S(t)}{\lambda f \, N(t)} = L(\theta) \ , \tag{4}$$

where

$$L(\theta) = \frac{\kappa}{\kappa - 1} \left(e^{-\theta} - e^{-\kappa\theta}\right) ,$$

$$\theta = l(t - t_0) ,$$

and

$$\kappa = \frac{m}{l} .$$

The relative leak rate, L, is shown graphically in Fig. 2.6 for a range of θ and for several values of the parameter κ.

Connection Between Release-Rate and Dose. The dose rate from airborne radioactive material is proportional to the air concentration of the material at or near the receptor point. The air concentration is, according to atmospheric dispersion formulas, proportional to the release rate with the condition that negligible time elapses between release and

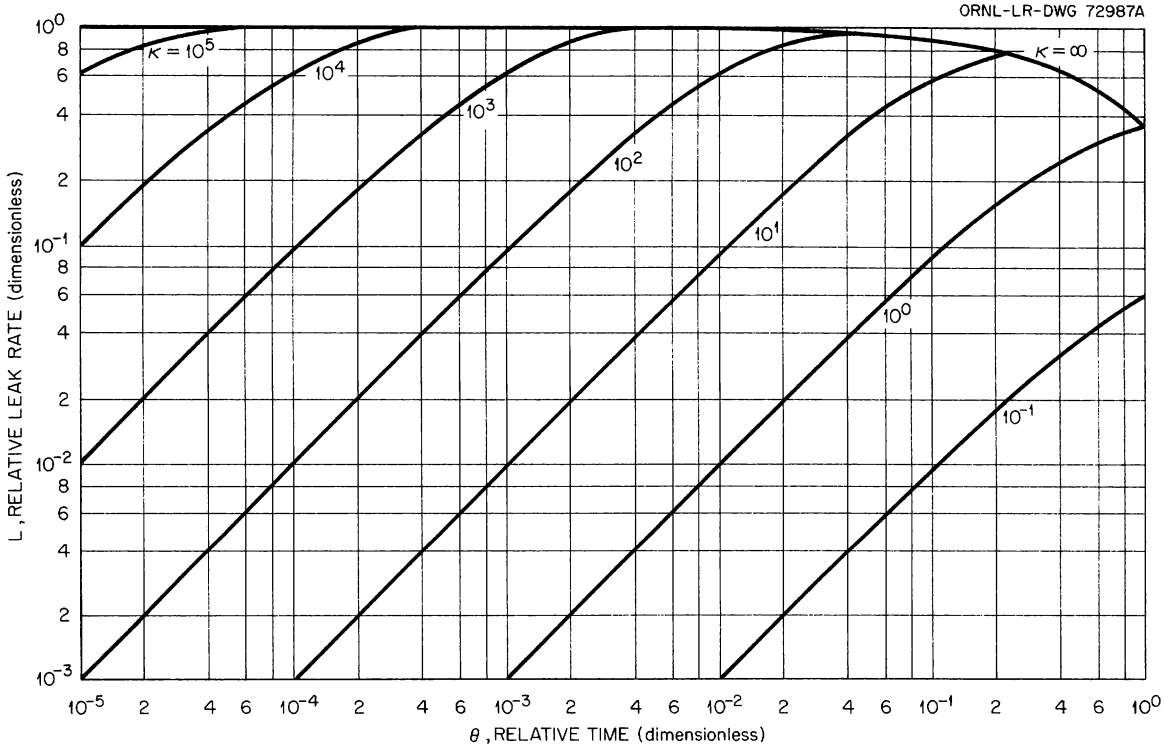

Fig. 2.6. Leak Rate from Double-Containment System with Step Release from Core of N.S. SAVANNAH Reactor.

arrival at the receptor point. The dose rate is, therefore, proportional to the release rate. For a given isotope the dose rate, $\dot{D}(t)$, is

$$\dot{D}(t) = K\, S(t) \ ,$$

where $S(t)$ is the release rate to the atmosphere and K is a time-independent quantity determined by the isotope under consideration, the atmospheric conditions, and the position of the receptor point relative to the release point. The dose, $D(t)$, up to time, t, is given by

$$D(t) = \int_0^t \dot{D}(\tau)\, d\tau = K \int_0^t S(\tau)\, d\tau \ . \tag{5}$$

Using Eq. (3) in Eq. (5) it is found that the dose, $D_1(t)$, from a single containment system with step release of material from the core is

$$D_1(t) = \lambda f K \int_{t_0}^{t} e^{-\lambda(\tau - t_0)}\, N(\tau)\, d\tau \ . \tag{6}$$

Similarly using Eq. (2) in Eq. (5) the double containment dose is seen to be

$$D(t) = \lambda f K \frac{\frac{\mu}{\lambda}}{\frac{\mu}{\lambda} - 1} \int_{t_0}^{t} \left[e^{-\lambda(\tau - t_0)} - e^{-\mu(\tau - t_0)} \right] N(\tau)\, d\tau \ . \tag{7}$$

Effect of N.S. SAVANNAH Double Containment on Noble Gas Dose. The use of two series-connected containment structures can effect a reduction in the exposure dose arising from a reactor accident. The extent of this reduction can be determined by taking the ratio of the dose with double containment to the dose with single containment. Using the step model of core release, the dose ratio given by dividing Eq. (7) by Eq. (6) is

$$\frac{D(t)}{D_1(t)} = \frac{\frac{\mu}{\lambda}}{\frac{\mu}{\lambda} - 1} \left[1 - \frac{\int_{t_0}^{t} e^{-\mu(\tau - t_0)}\, N(\tau)\, d\tau}{\int_{t_0}^{t} e^{-\lambda(\tau - t_0)}\, N(\tau)\, d\tau} \right] . \tag{8}$$

From Eq. (8) it is seen that the reduction in dose depends on N(t) as well as the leak characteristics of the containment structures.

The noble-gas dose reduction resulting from compartment holdup in the N.S. SAVANNAH was investigated using three different compartment exhaust rates, and the results are shown in Fig. 2.7. The data of Fig. 2.7 were calculated using Eq. (8). It was assumed that the gases would be released from the core instantaneously at the start of the accident ($t_0 = 0$ in Eq. 8). The time-dependent amounts of the noble gases were calculated on the basis of reactor operation at full power for one year.[8] To account for possible nonuniform mixing in the reactor compartment, the compartment leak-rate constant, given by

$$m = \frac{\text{ventilation rate}}{\text{volume ventilated}} ,$$

was computed using approximately one-half the actual compartment volume.

---

[8]T. D. Anderson et al., Activity Release from the N.S. SAVANNAH in the Maximum Credible Accident, USAEC Report ORNL-3361, Oak Ridge National Laboratory, Oct. 1, 1963.

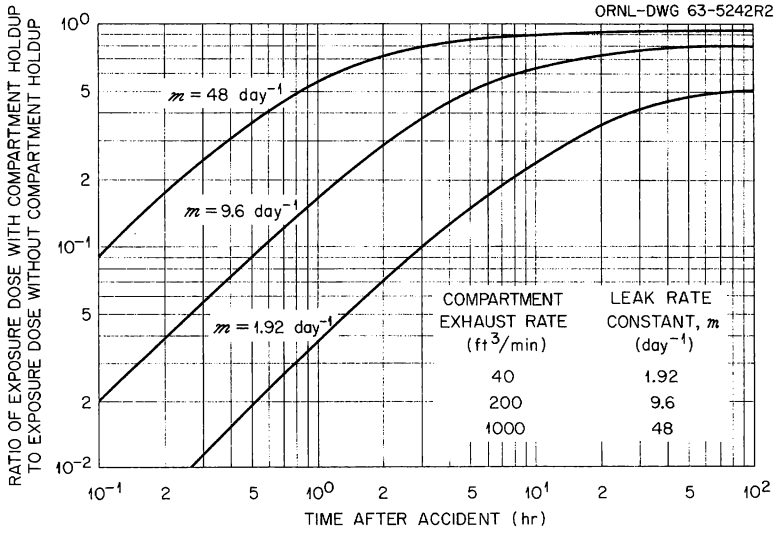

Fig. 2.7. Effect of Reactor Compartment Holdup on Dose from Noble Gases from N.S. SAVANNAH Reactor in the Event of the Maximum Credible Accident.

Figure 2.7 is valid for any primary containment leak-rate constant, l, in the range $0 < l \lesssim 0.025$ day^{-1}.

During initial operation of the N.S. SAVANNAH the emergency ventilation system was operated at an exhaust rate of 200 ft^3/min (m = 9.6 day^{-1}). At this exhaust rate the 2-hr dose from noble gases released to the atmosphere would be reduced 71% because of compartment holdup. The reduction in the infinite-time noble gas dose would be 20%. As can be seen from Fig. 2.7, a further reduction in noble gas dose could be effected by reducing the exhaust rate. At an exhaust rate of 40 ft^3/min the 2-hr dose would be reduced 93%, and the infinite-time dose would be reduced 50%. There is, of course, a lower limit on the exhaust rate because the reactor compartment must be maintained at subatmospheric pressure to assure effective operation of the filters and charcoal adsorbers. The results of this analysis show, however, that it would be desirable to reduce the compartment exhaust rate to the lowest possible value consistent with the negative pressure requirement.

Effect of Particle Agglomeration on the Penetration of Filters in Double Containment Systems (W. E. Browning, Jr., M. H. Fontana)

The penetration of filters by fission products adsorbed on submicron particulate matter has been of some concern to those responsible for the performance of nuclear containment systems employing filtration as a means of limiting activity release. The efficiency of absolute particle filters is specified to be greater than 99.95% for particles of 0.3-μ diameter, but the filtration efficiency is not known, with comparable certainty, for particles of substantially smaller size; for example, in the range 20 to 40 A. It is known, however, that particulate matter of high particle-count density per unit volume, as would exist after a reactor accident, would agglomerate at a rapid rate to yield a smaller number of larger particles.

A simplified calculation was performed to determine the effect of particle agglomeration on the activity release from a containment system that depends on particulate filtration for its effectiveness. The case treated here is that of a dispersion of activity into a primary volume, such as the first containment vessel, and its leakage into a secondary

volume in which a sweep air flow is maintained and filtered before being exhausted into the surroundings. The secondary barrier is thus made effective in that all leakage from the surroundings flows into it and all activity that is released is filtered. Examples of this kind of containment are the N.S. SAVANNAH and the Hallam reactor systems.

The calculation of particle agglomeration was based on a simplified model that can be shown to be conservative. Since iodine is of major concern in filtration problems, it was chosen to illustrate the particle behavior. Only the particulate form of iodine was treated, and it was assumed that iodine remaining in vapor form was removed by adsorbers. The analysis was performed in the following manner. (1) It was assumed that all the iodine isotopes existing in the reactor core after full-power full-life operation were released at the time of the accident and evenly dispersed within the primary containment vessel as an infinite number of infinitely small particles. (2) The iodine was assumed to agglomerate as a monodisperse pseudoaerosol of pure iodine, and the particle size was computed as a function of time. (3) All the aerosol having a particle size less than 0.3 μ that leaked out of the primary containment vessel was assumed to penetrate the secondary containment filtration system. (4) The amount of iodine being released during this period of zero filter efficiency was calculated.

The agglomeration calculations were performed using the relationship[9]

$$\frac{1}{n} = \frac{1}{n_0} + Kt \ , \qquad (9)$$

where

n = number of particles per cm^3 at time t (cm^{-3}),

n_0 = number of particles per cm^3 initially (cm^{-3}),

t = time (sec),

K = agglomeration coefficient (cm^3/sec), taken as 5×10^{-10} (ref. 10).

---

[9]H. L. Green and W. R. Lane, Particulate Clouds, Dusts, Smokes, and Mists, pp. 126 et seq., E. and F. N. Spon, Ltd., London, 1957.

[10]W. H. McAdams, Heat Transmission, p. 172 (Eq. 7-4a), 3rd ed., McGraw-Hill, New York, 1954.

The value n was related to the concentration of matter in air by the equation

$$\frac{m}{V_1} = \rho \frac{\pi}{6} d^3 n \ , \tag{10}$$

where

m = total mass of material making the particles (g),

V_1 = total free volume of the primary containment vessel (cm^3),

ρ = density of the particle (g/cm^3),

d = diameter of particle (cm).

Substituting Eq. (10) into Eq. (9) yields the time required to reach a given diameter:

$$t = \frac{d^3 \pi \rho}{6 \frac{m}{V_1} K} - \frac{1}{n_0 K} \ . \tag{11}$$

Since n_0 is large, the last term is negligible.

The diluting effect of the sweep gas in the secondary containment vessel was considered because the filters were located in this system. The ratio of the rate of activity released from the secondary containment vessel to the activity release rate from the primary containment vessel can be shown to be

$$\frac{C_2 Q_{23}}{C_1 Q_{12}} = 1 - e^{-(Q_{23}/V_2)t} \ , \tag{12}$$

where

C_2 = concentration of material of interest in the secondary containment vessel ($curies/cm^3$),

Q_{23} = sweep gas volumetric flow rate (cm^3/sec),

C_1 = concentration of activity in primary containment vessel ($curies/cm^3$),

Q_{12} = volumetric leak rate from the primary containment vessel (cm^3/sec),

V_2 = volume of secondary containment vessel (cm^3).

The integrated release from the secondary containment vessel up to time t compared with the rate of release from the primary containment vessel is

$$\frac{A_{23}}{IR} = t - \frac{V_2}{Q_{23}} \left[1 - e^{-(Q_{23}/V_2)t}\right], \qquad (13)$$

where

A_{23} = total integrated activity released to time t (curies),

I = total activity inventory in the primary containment vessel available for release (curies),

R = primary containment vessel release rate (%/sec).

The particle size is shown in Fig. 2.8, which is based on Eq. (11), as a function of time for seven values of (m/V_1) and a particle density of 4.93 g/cm^3, corresponding to elemental iodine. Curve E shows the values for the N.S. SAVANNAH. Figure 2.9 shows the performance of the secondary containment vessel sweep gas system by relating the total activity released to time t for three values of the volume change time (V_2/Q_{23}). Curve E of Fig. 2.8 is superimposed on Fig. 2.9 to show the procedure for finding the worst case for operation of the system, assuming that all activity, I, is in particulate form and all that is released from the primary containment vessel prior to the time that the critical particle size is attained passes through the filtering system in the secondary containment vessel. For example, if 0.3 μ is chosen as the critical particle diameter, it can be seen that if the core inventory of iodine is the only material available to make particles, this size will be reached in 235 sec. The N.S. SAVANNAH has a secondary containment volume change time of 900 sec, and this curve shows that the total release to the atmosphere is $A_{23}/I = 26R$. Since the N.S. SAVANNAH primary containment has a maximum leakage rate of 3%/day,

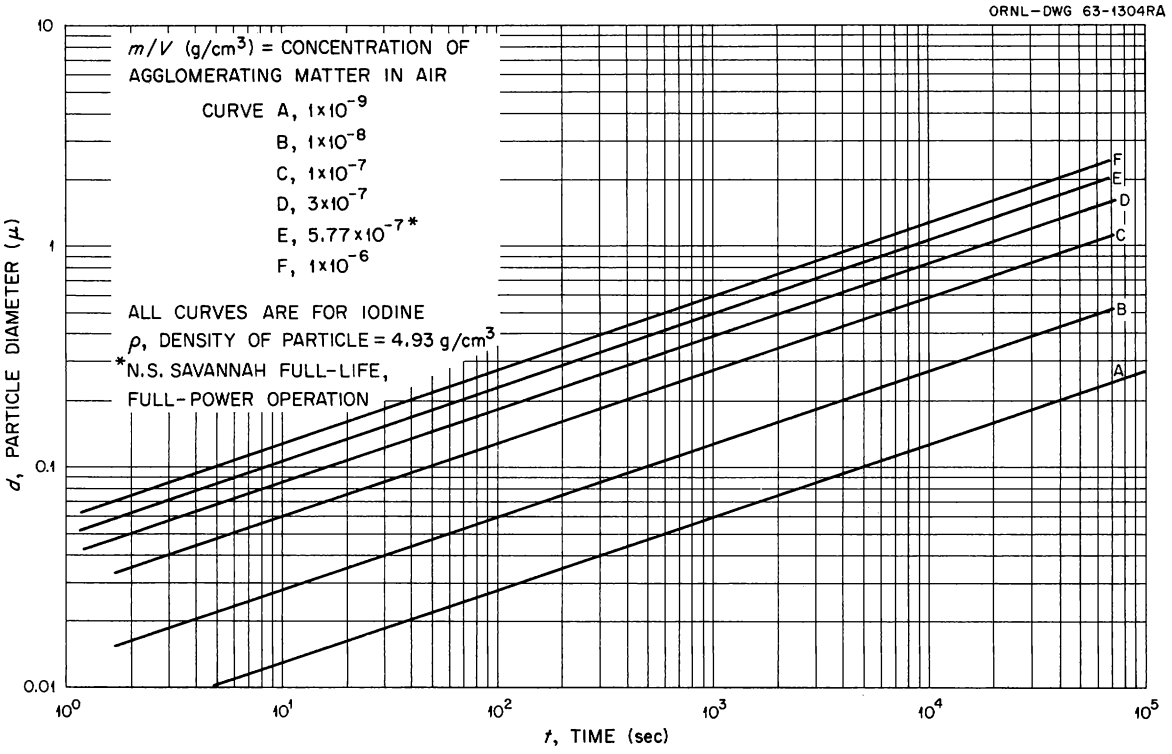

Fig. 2.8. Particle Size vs Time for Various Concentrations of Agglomerating Matter in Air.

$$R = \frac{0.03}{8.65 \times 10^4} \text{ sec}^{-1} = 3.47 \times 10^{-7} \text{ sec}^{-1} ,$$

and the ratio of total activity released to that available is

$$\frac{A_{23}}{I} = 26(3.47 \times 10^{-7}) = 9.02 \times 10^{-6} .$$

Table 2.6 shows the core inventory and amounts released to the surroundings for the N.S. SAVANNAH for the case of a 0.3-μ critical aerosol diameter.

This analysis of the effect of agglomeration is based upon established principles or upon assumptions that are clearly pessimistic. Equation (9) has been shown to hold ever since reliable methods of counting the particles in smoke clouds have been available.[9] Theoretical expressions for coagulation of monodisperse particles can be shown to take the

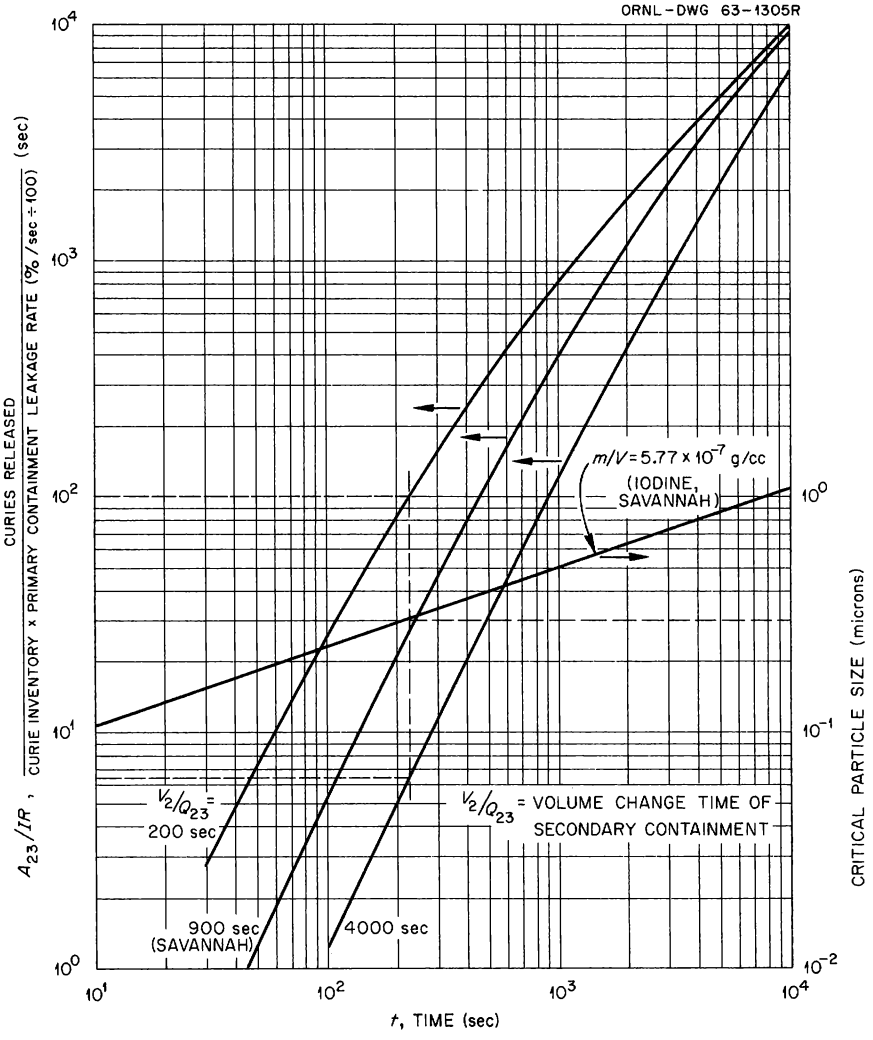

Fig. 2.9. Performance of Secondary Containment Vessel Sweep Gas System.

Table 2.6. Activity Release Under the N.S. SAVANNAH Accident Conditions Based on a 0.3-μ Critical Aerosol Diameter

Nuclide Released	Core Inventory (curies) After 600 Days at 69 Mw	Amount Released (curies)
8.05d ^{131}I	2.29×10^4	0.206
20.8h ^{133}I	2.05×10^6	18.5
6.68h ^{135}I	2.01×10^7	181

form

$$\frac{1}{n} - \frac{1}{n_0} = \frac{4RT}{3\eta N}\left(1 + \frac{A\ell}{r}\right) t \ , \qquad (9a)$$

where

R = gas constant,

T = absolute temperature,

η = viscosity of the medium,

N = Avagadro's number.

The term $1 + (A\ell/r)$ is the Cunningham correction for non-Stokes behavior of very small particles, where A is a constant (~0.9), ℓ is the mean free path of the molecule, and r is the radius of particle. From Eq. (9a) it can be seen that the coagulation coefficient,

$$K = \frac{4RT}{3N}\left(1 + \frac{A\ell}{r}\right) ,$$

would decrease as the radius increases. Experimentally determined graphs of t vs 1/n are straight lines within the limits of experimental error, except for the case of very small particles for which there is an indication of curvature. The use of this theoretical expression for K for air at standard conditions and a standard stearic acid cloud yields $K = 5.1 \times 10^{-10}$ cm^3/sec. The use of $K = 5.00 \times 10^{-10}$ cm^3/sec in this analysis in Eq. (9) appears justified on a conservative basis.

The artifice of assuming that all the iodine coagulates into particles of pure iodine is a useful concept that can be shown to be conservative. Actually, in the case of a real accident, some of the iodine would remain in the vapor form and some would deposit on particles caused by debris and smoke concurrent with fuel meltdown. Taking the case of all the iodine depositing on particles of other matter, the m of Eq. (11) must include the iodine plus the other debris and must be larger than the case of pure iodine; for example,

$$m_t = m_0 + m_1 \ , \qquad (14)$$

where

m_t = total mass (g),
m_0 = mass of foreign matter (g),
m_1 = mass of iodine (g).

It can be seen from Eq. (11), however, that the time required to reach a critical filterable diameter is directly proportional to ρ_t/m_t. Since $\rho_t/m_t = 1/V_p$, where V_p is the volume taken up by the particle, substitution into Eq. (11) shows that

$$t = \frac{d^3\pi}{6K\frac{V_p}{V_1}} ; \qquad (11a)$$

that is, the time to reach a given diameter is inversely proportional to the ratio of the volume taken up by the particles to the total free volume of the containment vessel. [Note, however, that V_p/V_1 must be very small for Eq. (9) to hold.] Equation (11a) shows that if foreign matter is added to the iodine, the time at which filtration becomes effective will be shorter.

The usual effect of a size distribution in a cloud of particles is to promote agglomeration at a faster rate than would occur in a cloud of equal-sized particles.[9] It appears that the faster agglomeration rate of the polydisperse particles and the assumption that all particles of a size below 0.3 μ penetrate the filter introduce a greater degree of conservatism to this worst case analysis than could be obtained by neglecting the trace amount of small particles that has not undergone agglomeration up to the time of filtration.

From the results of this simplified analysis, it appears that the extent of fission-product penetration of filtration units by transport of particulate matter may be limited because, with the high particle-count density which would exist after a catastrophic reactor accident, the particles would agglomerate in a very short time to a size readily removable by filters. This analysis shows that agglomeration would occur at a rate fast enough to prevent significant penetration of the filtration

systems, even if all particles of a size smaller than 0.3 μ were assumed to penetrate the filters. In one example, the calculated amount of iodine released would be less than 10^{-5} of that available.

Spent Fuel Temperatures Following Loss of Coolant from Transfer Cask (O. H. Klepper)

Refueling of the N.S. SAVANNAH reactor will require transferring the spent fuel from the ship to the shore fuel-handling facility. This transfer is to be made in a transfer cask with a capacity of one fuel element. During normal cask operation the spent fuel element will be immersed in water that will transport the fission-product decay energy by natural convection to a secondary water cooling system. Should the water be lost from the cask during the transfer, the fuel would become hotter, since the decay heat would have to be transported mainly by radiation and air convection from the fuel to the cask wall and on to the atmosphere. Under these circumstances it becomes of interest to know the temperature distribution within the cask, since this might affect the integrity of the cask and of the fuel. Should the fuel cladding fail, knowledge of the fuel temperature will be needed to assess the release of fission products from the fuel. In view of these considerations, an estimate of transfer cask temperatures following simultaneous loss of primary and secondary coolant from the cask was made.

A number of the factors that affect the process of heat removal from the cask are not well known at the present time. The emissivity of the cask internals and of the fuel, the extent to which the lead in the cask is bonded, and the external environment that the cask might be exposed to all fall into this category. Where convenient, these uncertainties were treated as variable parameters so that direct application of the results can be made once a specific value of the parameter is known. Consideration of other uncertainties had to be deferred.

Heat Removal Process Following Loss of Coolant. The spent fuel consists of 0.5-in.-OD stainless steel-clad fuel pins with an active length of 66 in. Each fuel element contains 164 fuel pins spaced 0.663 in. center-to-center in a rectangular array. The pins form a fuel element approximately 8.5 in. square and 66 in. long. Inside the cask the

fuel element is enclosed by a central, box-shaped, stainless steel liner about 0.25 in. thick (Fig. 2.10). Approximately 0.25 in. clearnace is provided between the fuel element and the liner. Following a loss of coolant from the cask, heat transfer from the fuel to the surrounding liner would be primarily by radiation. The energy adsorbed by the liner would, in turn, be transferred to the stainless steel guide tube (~14 in. ID, 15 in. OD) that surrounds the liner. The average clearance between the liner and the guide tube is about 1.65 in. This heat transfer would be primarily by radiation and air convection. The next step in the outward heat flow would be from the guide tube to the mild steel wall of the cask cavity across an additional air gap of about 0.5 in. Here again the prime transfer mechanisms would be radiation and natural convection. The cask wall consists of an inner cylindrical mild steel shell about 1 in. thick and 16 in. ID, with an outer cylindrical mild steel shell about 2 in. thick and 42 in. OD. The approximately 10-in. annular space between the shells contains lead shielding. The heat flow through the wall to the cask exterior surface would be primarily by conduction, except at the interfaces between lead and steel, as will be discussed later. Heat transfer from the cask to the atmosphere was assumed to be only by natural convection.

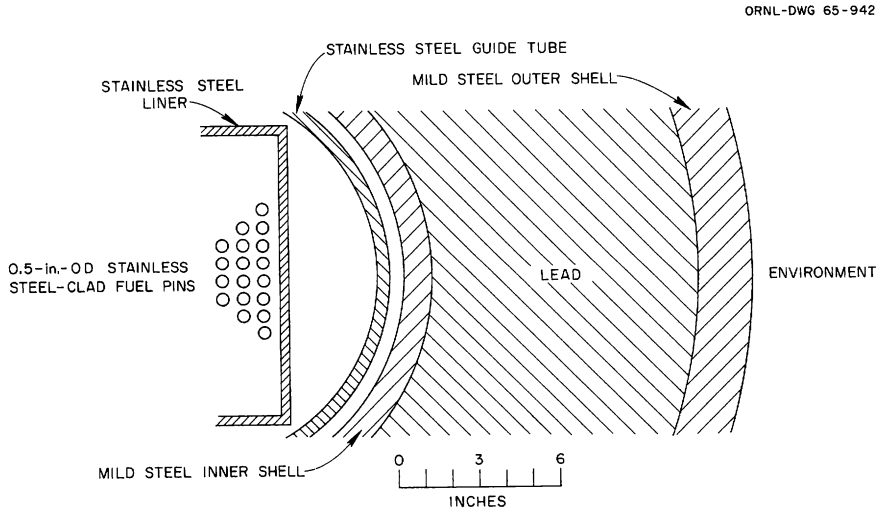

Fig. 2.10. Configuration of Fuel Transfer Cask.

Heat Generation. Fuel element heat generation from the decay of fission products was computed according to the Way-Wigner formulation. The following assumptions were made in this calculation: (1) reactor operation at 63.5 Mw(t) for 100 days preceding shutdown and (2) a radial power peaking factor of 2.0 and an axial power peaking factor of 1.5 for the central, and hottest, fuel element. The peak heat-generation rate for the central fuel element is plotted in Fig. 2.11.

Heat Transfer from the Cask to the Environment. The primary heat exchange mechanisms are convection and radiation. Thermal radiation will depend on the temperature and the emissivity of the surroundings. Radiant heat loss to the surroundings was ignored because the required information on ground conditions, etc. was not available. This error is conservative, since it would tend to raise the calculated cask temperatures. Solar radiation might increase cask surface temperatures by about 50°F

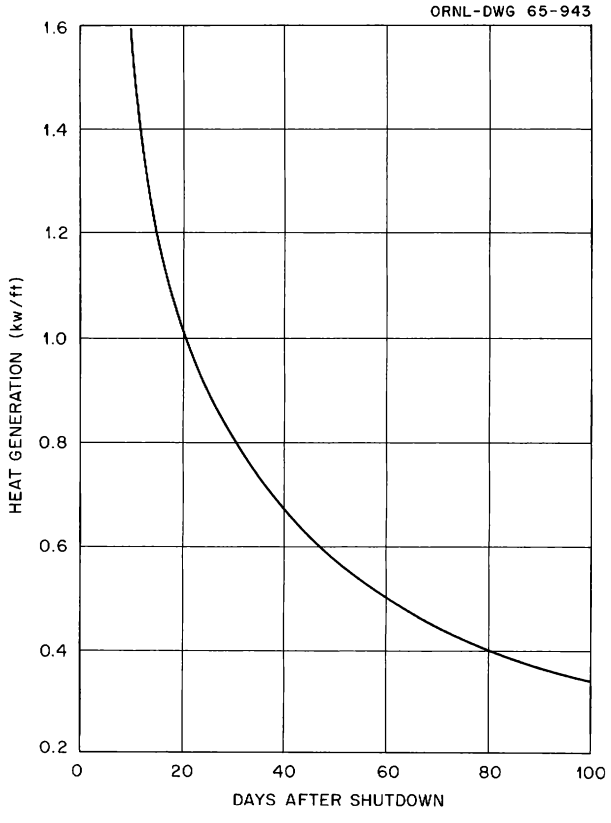

Fig. 2.11. Peak Decay Heat Generation for Central Fuel Element.

and increase cask interior temperatures by a lesser amount. Again, this effect was ignored because the amount of exposure to the sun is uncertain. The convection heat transfer calculation was based on the full cask height of 9.4 ft being effective with the cask in the upright condition. Subsequent calculation of the heat transfer between the liner and the cask wall showed that the upright position results in higher cask temperatures than the horizontal position. The ambient air temperature was assumed to be 100°F, and the heat transfer coefficient was obtained from ref. 11. Cask surface temperatures decreased from 250°F at 10 days after shutdown to about 150°F at 100 days after shutdown.

Heat Transfer Through Cask Wall. The cask wall consists of an outer mild steel shell approximately 2 in. thick, a concentric inner mild steel shell about 1 in. thick, and about 10 in. of lead cast in place between the shells. The lead was not bonded to the supporting steel, and therefore an air gap may separate the lead from the steel. This possibility was taken into account by assuming a 0.1-in. air gap between the lead and the outer cask shell. The temperature drop across the cask wall was calculated to be about 120°F at 10 days after shutdown and about 25°F at 100 days after shutdown. The corresponding values based on contact between lead and steel are 15°F and 3°F, respectively. It appears therefore that the lead will stay well below its melting point of about 620°F.

Heat Transfer from Liner to Cask Wall. Two steps are involved in heat transfer from the liner to the cask wall; that is, there is heat transfer from the liner to the guide tube and then from the guide tube to the cask wall. Convection and radiant heat transfer are significant in both steps. The liner and the guide tube are relatively thin, so axial heat transfer in these two components was ignored. The liner is box shaped, with sides approximately 9.5 in. wide, and the surrounding guide tube has an inside diameter of about 14 in. For calculational purposes the liner was assumed to be an equivalent cylindrical surface concentric with and interior to the guide tube, and the air gap between the two was taken to be 1.65 in. wide. Convection heat transfer was determined in accordance with ref. 11. The calculations showed that the

---

[11]Ibid., p. 181 (Eq. 7-9b).

convection heat transfer coefficient for vertical annular spaces was smaller than one for horizontal annular spaces. The highest fuel element temperatures would therefore be expected with the cask in a vertical position, so this case was analyzed.

Radiant heat transfer from the liner to the guide tube and from the guide tube to the inner cask surface was calculated in accordance with ref. 12. The emissivity of the mild-steel cask wall was taken as 0.7, a reasonable value for oxidized steel. Since the surface condition of the stainless steel liner and that of the guide tube are not well known, two cases were treated with emissivities of 0.5 and 0.7, respectively, where the lower value may correspond to the as-received condition. Liner temperatures ranged from about 900°F at 10 days after shutdown to about 470°F at 100 days when the liner and guide tube emissivities were taken as 0.7. These temperatures were increased by 100°F and 50°F, respectively, for emissivities of 0.5. If no contact between the lead and the outer cask shell is assumed, the liner temperature is increased by approximately 20°F. The small temperature gradients across the liner and guide tube walls were neglected in these calculations.

Heat Transfer from Fuel to Liner. Convection heat transfer should be minor within the fuel element because of the small clearance between the fuel pins. Conduction heat transfer too should not be important at temperatures sufficiently high to be of concern. Radiant heat transfer is therefore the prime mechanism for removing decay heat.

The computer method described in ref. 13 was used to estimate the temperature distribution within the element. The radiant interchange factors required by that method were obtained from ref. 14. Axial conduction heat transfer within the fuel pins was shown to be minor, and

---

[12]W. H. Giedt, Principles of Engineering Heat Transfer, p. 259 (Eq. 13.21), Van Nostrand, New York, 1957.

[13]J. S. Watson, Heat Transfer from Spent Reactor Fuels During Shipping: A Proposed Method for Predicting Temperature Distribution in Fuel Bundles and Comparison with Experimental Data, USAEC Report ORNL-3439, Oak Ridge National Laboratory, May 27, 1963.

[14]O. H. Klepper, Radiant Interchange Factors for Heat Transfer in Parallel Rod Arrays, USAEC Report ORNL TM-583, Oak Ridge National Laboratory, Dec. 26, 1963.

this effect was therefore ignored. The emissivity of the fuel cladding after exposure to the primary system is not well known. An emissivity measurement of stainless steel tubing in the as-received condition is reported as 0.55 in ref. 13. The crud deposited on pressurized-water reactor fuel would be expected to increase the emissivity somewhat, but it is difficult to predict how much. In an attempt to cover the emissivity range of interest, fuel temperatures were calculated for cladding emissivities of 0.5, 0.7, and 0.9. The liner surface facing the fuel was also assumed to have these emissivities.

Peak Fuel Temperatures. Cladding temperatures for the center pin of the central fuel element are shown in Fig. 2.12 as a function of time after shutdown. Depending on what assumptions are made concerning lead bonding and emissivities of the various components, peak cladding temperatures range from 1220 to 1540°F at 10 days after shutdown. The corresponding temperatures at 100 days are 730 to 880°F. It is noted that the degree of contact between the lead and steel in the cask wall has a rather minor effect on cladding temperature, increasing it no more than 25°F. The emissivities of the guide tube and of the liner surface facing it have a somewhat larger impact, increasing cladding temperatures by as

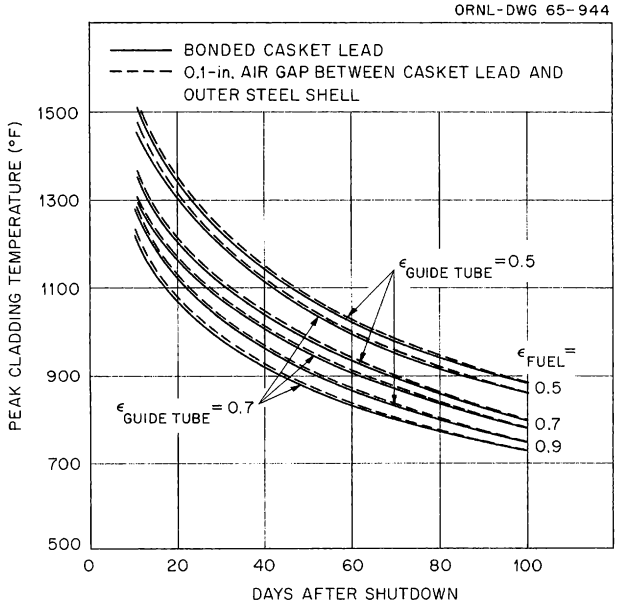

Fig. 2.12. Peak Cladding Temperature of Central Fuel Element.

much as 60°F for a decrease in emissivity from 0.7 to 0.5. The emissivity of the fuel cladding affects the peak temperature even more, increasing it about 170°F for a decrease in emissivity from 0.7 to 0.5 at 10 days after shutdown. For increasingly longer times after shutdown the temperature effect of the above-mentioned factors of course becomes less. While the cited temperatures were calculated for the cladding surface, it is expected that the centers of the fuel pins will be only slightly hotter at the prevailing low heat generation rates.

It is thought that these fuel cladding estimates were made by fairly conservative calculational methods. However, several other minor factors not accounted for in the calculation will tend to reduce the temperatures. Among these are (1) the heat transport by gamma radiation that will transfer about 15% of the decay heat from the fuel to beyond the inner cask wall surface, (2) axial heat transfer in the fuel-liner-guide tube region, and (3) convection heat transfer inside the fuel bundle and between the fuel and the liner. Among effects that might increase the calculated temperatures are solar heating and, possibly, fire. These conditions should be assessed when sufficient information becomes available.

Port Survey Visits (S. I. Kaplan)

The AEC mandate governing operation of the N.S. SAVANNAH continues to specify that before the ship may enter a port, a survey of the port must be conducted in order to select a berth meeting the N.S. SAVANNAH site requirements and to establish an emergency plan for removing the ship in case of an accident. A report of the survey is filed with the AEC Office of Regulation for approval prior to the ship's arrival. The team performing the survey has generally consisted of one or more senior deck officers from the SAVANNAH staff and a nuclear engineer from ORNL.

After completing its first tour of U.S. ports[15] and proceeding to its maintenance base at Galveston, the vessel was scheduled to visit several coastal cities in northern Europe and the eastern U.S., commencing

[15]S. I. Kaplan, Port Survey Visits, pp. 32–38, Maritime Reactor Program Ann. Progr. Rept. Nov. 30, 1962, USAEC Report ORNL-3416, Oak Ridge National Laboratory.

in May 1963. Surveys made in anticipation of the voyage covered the ports of Hamburg, Bremerhaven, Oslo, Copenhagen, Southampton, Baltimore, Boston, and New York; in addition, preliminary talks describing the conduct and intent of a port survey were held in Antwerp and Rotterdam at the request of EURATOM officials.

Linear-Worth Control Rod Program

S. I. Kaplan

In 1961, at the request of the AEC-Maritime Administration Joint Group, a control rod positioning program was prepared for use with N.S. SAVANNAH core I and the replacement rod drive system being developed by the Marvel-Schebler Division of Borg-Warner Corporation. The intent of this program was to facilitate manual adjustment of reactivity by providing an essentially linear relationship between rod travel and reactivity change. The scheme was developed by using critical experiment data and calculated reactivity coefficients and by assuming a symmetrical axial flux distribution. During the subsequent operation of the ship, physics measurements were made that yielded data sufficiently different from the original assumptions to warrant recomputing the program; accordingly, a revised program was prepared and submitted in January 1963.

The reactivity control technique used with the present rod drive system is to bring the reactor critical by withdrawing symmetrical four-rod banks, one at a time, commencing at the core periphery and working toward the center. This outside-in pattern is modified in the range of appreciable power output by withdrawing a bank of high worth (the A bank) to its mid-position so that an adequate rate of reactivity change is always available to the operator to meet maneuvering requirements. As load and burnup conditions change, the other rods are positioned as necessary to permit maintaining the A bank in its most effective working range.

A reactivity change rate equivalent to that of the A bank can also be produced by moving other banks in the normal sequence, provided more than one bank is moved simultaneously. The sequence controller incorporated in the replacement drives can be programmed to withdraw and insert the 21 rods in an overlapping pattern such that the desired rate of

reactivity change is achievable over most of the available rod movement; hence fuel-maneuvering capability can be utilized by the operator throughout core life, without altering the sequence of rod positioning.

The final scheme was constructed by superposing curves of worth versus position for the various banks until an approximately linear relationship with the desired slope over the working range resulted. The individual banks worths measured in shipboard physics experiments are shown in Table 2.7. It was observed that although the bank worth curves were asymmetric and the worth of a given bank varied according to the disposition of the other banks, the curve shapes fell basically into two groups: (1) those in which the A rods were banked in a partially withdrawn position and (2) all others. Using the total clean-core worth of $14.40 and the holddown margin of $2.90 observed in the zero-power experiments,[16] effective rod bank worths for the desired outside-in withdrawal pattern were estimated from the runs in Table 2.7. The shapes of the worth curves were taken to match experimental data taken from Table 2.7, as follows:

Rod Bank	Run No.	Estimated Worth ($)
E	1	2.15
D	2	3.15
C	5	3.70
B	8	3.80
A	8	3.50
X	8	1.00

Figure 2.13 shows the final pattern and predicted behavior with an average slope of $\sim 1.47 \times 10^{-3}$ δk/in., corresponding to a reactivity addition rate of 2×10^{-2} δk/min at the maximum rod withdrawal speed of 13.5 in./min. Conversion from dollar units of reactivity to δk_{excess} was based upon a delayed neutron fraction $\beta = 0.00751$ (ref. 17). The projected

[16] R. M. Ball and A. L. MacKinney, Nuclear Merchant Ship Reactor, Zero Power Test, Core I, USAEC Report BAW-1202, Babcock & Wilcox Co., June 1960.

[17] R. E. Wascher, N.S. SAVANNAH Replacement Control Rod Drives, Safeguards Report, Vol. II, para. 4.2.1.2, USAEC Report BAW-1249, Babcock & Wilcox Co., October 1962.

Table 2.7. Comparison of Experimental Rod Bank Worths for Various Configurations

Run No.	Rod Bank	Positions of Other Rods[a]	Total Worth ($)	Measurement Method	Fraction of Total Worth At[a]				
					10 in.	20 in.	30 in.	40 in.	50 in.
1	E	All at 0	2.15	Subcritical multiplication	0.07	0.25	0.62	0.84	0.97
2	D	E at 58 in.; others at 0	3.70	Moderator temperature	0.07	0.28	0.68	0.85	0.98
3	D	E at 58 in.; A at 28 in.; C,B,X at 0	2.70	Moderator temperature	0.13	0.44	0.73	0.90	0.98
4	D	E at 58 in.; A at 25.5 in.; C,B,X at 0	2.81	Moderator temperature	~0.13	0.46	0.72	0.89	0.98
5	C	E,D at 58 in.; A,B,X at 0	4.35	Moderator temperature and power coefficient	0.09	0.33	0.67	0.85	0.97
6	C	E at 58 in.; D at 4.5 in.; A at 25.5 in.	4.00	Moderator temperature	0.18	0.56	0.81	0.94	0.98
7	A	E at 58 in.; D at 58–31 in.; C at 30–0 in.; B,X at 0	4.35	Period 508°F	0.13	0.45	0.70	0.88	0.97
8	A	E at 58 in.; D at 35.6 in.; C,B,X at 0	4.15	Moderator temperature	0.11	0.39	0.68	0.86	0.96
9	X	E at 58 in.; D at 40.3–30.5 in.; C,B,A at 0	0.65	Period 346°F	0.08	0.33	0.63	0.86	0.97
10	X	E at 58–45 in.; D at 16.5–0 in.; C,B,A at 0	1.00	Period 89°F	0.07	0.28	0.53	0.77	0.95
11	X	E at 58 in.; D at 58–10.3 in.; C at 9.9–0 in.; A at 30.5 in.; B at 0	2.57	Period 508°F	0.14	0.52	0.86	0.97	1.00
12	Idealized				0.10	0.38	0.68	0.90	0.97

[a]Rod positions given in inches withdrawn from fully inserted position.

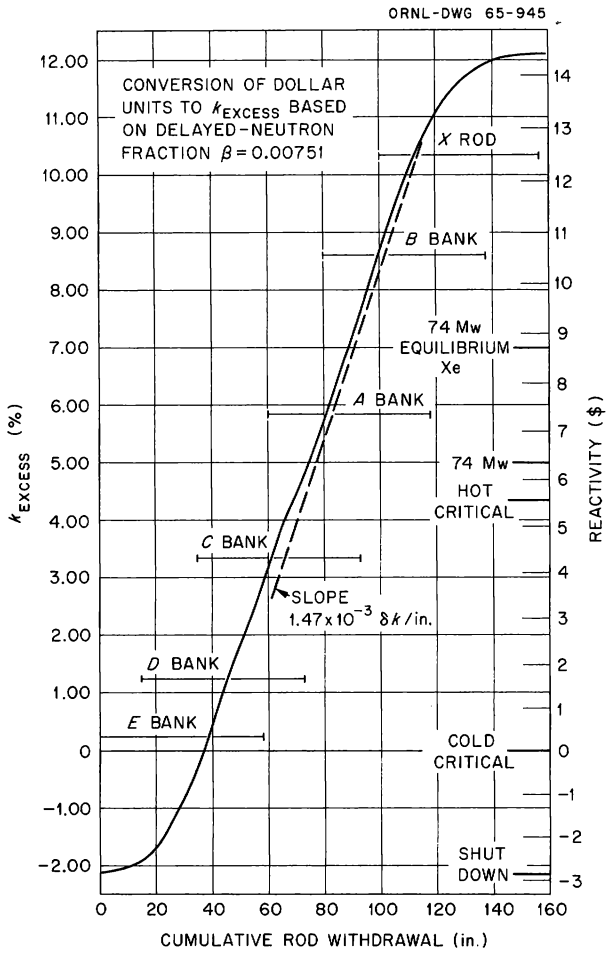

Fig. 2.13. Linear-Worth Control Rod Program for N.S. SAVANNAH.

reactivity introduction rate is adequate to assure full maneuvering capability of the ship and is well below the maximum safe rate; this latter was found to be in excess of 6×10^{-2} δk/min in analog computer studies of the reactor.[18]

The scheme shown in Fig. 2.13 is intended as a basis for initial sequence-controller settings to be verified and revised empirically by actual shipboard experiments. Because the effective rod bank worths change continuously as adjoining rods are displaced, a digital computer solution is not considered to guarantee results superior to the graphical estimate obtained. Once the settings up to the full-power equilibrium-xenon level are determined, however, the settings for the remaining core

[18]Ibid., para. 4.2.2.2.

life can be predicted by assuming an invariant shape for the inner rod worth curves (e.g., Table 2.7, Run 12) and calculating the effective rod pattern worth at several increments of withdrawal. The new overall rod worth curve thus generated can then be compared with the experimentally verified program and adjusted and recalculated, if required, to match the desired slope. Calculations of rod worths for the N.S. SAVANNAH using the presently-employed bank-to-bank sequence were made[19] that yielded rod worth curves which compare favorably with experimental values.

---

[19]E. E. Gross, M. L. Winton, B. W. Colston, Lifetime Studies for the N.S. SAVANNAH Reactor, USAEC Report ORNL-3261 (supp.), Oak Ridge National Laboratory, March 1963.

3. ADVANCED CORE DEVELOPMENT

Boron Burnable Poison Study

T. D. Anderson E. E. Gross
M. L. Winton

Previous studies[1,2] indicated that the reactivity lifetime of the N.S. SAVANNAH core I fuel elements would be increased about 60% by replacing the stainless steel fuel-element containers with a similar Zircaloy structure. This indicated increase in reactivity lifetime stimulated further studies[3] in which boron burnable poison was added to the stainless steel fuel tubing. The main goal of the burnup studies was to determine approximate fuel and burnable poison loadings required for various reactivity lifetimes. With this information an economic analysis giving the general trend of fuel-cycle costs with core life was made. Some problems associated with long-lived cores were also studied.

The N.S. SAVANNAH core I is described in other reports,[1,3,4] and will not be described here.

Burnup Studies with Simplified Model

The results reported in this section were obtained by using the following simple expression for the multiplication factor as a function of

---

[1]E. E. Gross, B. W. Colston, and M. L. Winton, Nuclear Analyses of the N.S. SAVANNAH Reactor with Zircaloy or Stainless Steel as Fuel-Element Containers, USAEC Report ORNL-3261, Oak Ridge National Laboratory, April 24, 1962.

[2]E. E. Gross, M. L. Winton, and B. W. Colston, Lifetime Studies for the N.S. SAVANNAH Reactor, USAEC Report ORNL-3261 (suppl.), Oak Ridge National Laboratory, March 18, 1963.

[3]T. D. Anderson, E. E. Gross, and M. L. Winton, Burnable Poison Studies for the N.S. SAVANNAH Reactor, USAEC Report ORNL-TM-716, Oak Ridge National Laboratory.

[4]G. E. Kulynych, Nuclear Merchant Ship Reactor Final Safeguards Report, Description of the N.S. SAVANNAH, USAEC Report BAW-1164, Vol. I, Babcock & Wilcox Co., June 1960.

time:

$$k(N^{25},N^{p},t) = \frac{aN_0^{25}\bar{\sigma}_0^{25}\, e^{-\beta t}}{b + N_0^{25}\bar{\sigma}_0^{25}\, e^{-\beta t} + N^{p}\bar{\sigma}_0^{p}\, e^{-(\bar{\sigma}_0^{p}/\sigma^{25})\,\beta t}}, \qquad (1)$$

where a, b, and β are constants,

N_0^{25} = initial atom density of ^{235}U in the core,
N_0^{p} = initial atom density of burnable poison in the core,
$\bar{\sigma}_0^{25}$ = initial flux-averaged ^{235}U cross section,
$\bar{\sigma}_0^{p}$ = initial flux-averaged burnable poison absorption cross section.

It may be seen that if space- and energy-averaged cross sections are used, Eq. (1) is in the form for expressing the probability of absorption in ^{235}U. The main assumptions inherent in Eq. (1) are that

1. The reactor is operated at constant power,
2. The variation of the flux in space and energy is time independent,
3. Only the atom densities of ^{235}U and of the burnable poison vary with time.

The justification and limitations of Eq. (1) may be seen by comparing the results obtained using Eq. (1) with results obtained using a more detailed model that does not rely on assumptions 2 and 3 above.

The starting point for the burnup calculations was the flux distribution obtained from detailed analyses of the beginning-of-life cores.[1] The flux distributions were used to obtain the space- and energy-averaged cross sections for ^{235}U and ^{10}B needed in Eq. (1). The cross sections for ^{10}B (in the fuel cladding) and for ^{235}U are given in Table 3.1.

Table 3.1. Space- and Energy-Averaged Absorption Cross Sections for ^{235}U and ^{10}B in Cores with Stainless Steel and Zircaloy Fuel-Element Containers

Fuel-Element Containers	$\bar{\sigma}_0^{25}$ (barns)	$\bar{\sigma}_0^{10}B$ (barns)
Stainless steel	43.0	241.7
Zircaloy	43.7	244.0

The three constants in Eq. (1) were determined from the following three conditions:

$$k(N_0^{25},0,0) = k_0 = \frac{aN_0^{25}\bar{\sigma}_0^{25}}{b + N_0^{25}\bar{\sigma}^{25}} , \tag{2}$$

$$k(N_1^{25},0,0) = k_1 = \frac{aN_1^{25}\bar{\sigma}_0^{25}}{b + N_1\bar{\sigma}_0^{25}} , \tag{3}$$

$$k(N_0^{25},0,T) = 1.000 = \frac{aN_0^{25}\bar{\sigma}^{25}\ e^{-\beta T}}{b + N_0^{25}\bar{\sigma}_0^{25}\ e^{-\beta T}} . \tag{4}$$

The multiplication factors, k_0 and k_1, are known from detailed calculations[1] on cores containing N_0^{25} and N_1^{25} ^{235}U atom densities, respectively. The lifetime, T, in Eq. (4) is taken from detailed burnup calculations[2] for cores with an initial loading of N_0^{25} ^{235}U atoms/cm^3 and no boron burnable poison. Thus Eq. (1) was force-fitted to data obtained by somewhat sophisticated methods. In this manner the values given in Table 3.2 for a, b, and β were obtained.

Table 3.2. Values of the Constants a, b, and β in Eq. (1) for Stainless Steel and Zircaloy Fuel-Element Containers

Fuel-Element Container	a	b	β
Stainless steel	1.3623	0.00295	0.1424
Zircaloy	1.5249	0.00376	0.1124

Equation (1), with ^{235}U cross sections from Table 3.1 and with values of a, b, and β from Table 3.2, is plotted in Fig. 3.1 for both stainless steel and Zircaloy fuel-element containers with initial fuel loadings containing 4.2 wt % ^{235}U fuel and no burnable poison. Also plotted in Fig. 3.1 are the burnup results from a more detailed calculation,[2] which were

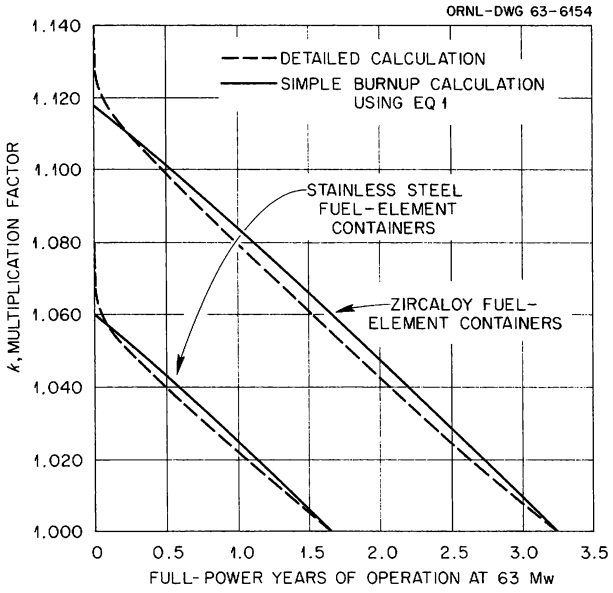

Fig. 3.1. Comparison of Calculated Reactivity Lifetimes for N.S. SAVANNAH-Type Cores Obtained by Using the Simplified and Detailed Models.

used to obtain the value of T in Eq. (4). Except for the initial buildup of xenon and samarium, the two calculations of the multiplication factor differ throughout core life by, at most, 0.004.

With the use of Eq. (1), cross sections from Table 3.1, and the values of a, b, and β from Table 3.2, the hot multiplication factor was calculated as a function of time for various fuel and poison loadings. For the purposes of this study the further restriction was added that each loading considered should provide the same shutdown margin that is provided in the original core I loading. This meant that at no time should the hot multiplication factor of Eq. (1) be greater than 1.06 for the core with stainless steel fuel-element containers and 1.11 for the core with Zircaloy fuel-element containers.[1] It was thus assumed that the control rod worth is independent of fuel and boron loadings.

Core lifetimes obtained using Eq. (1) with the above limitations on shutdown margin are shown in Fig. 3.2 with the required fuel and ^{10}B loadings. It is interesting to note that with a reasonable load factor of 0.67, the longest core life considered (~6 full-power years) would allow two core loadings to serve out the usual 20-year life expectancy of a ship.

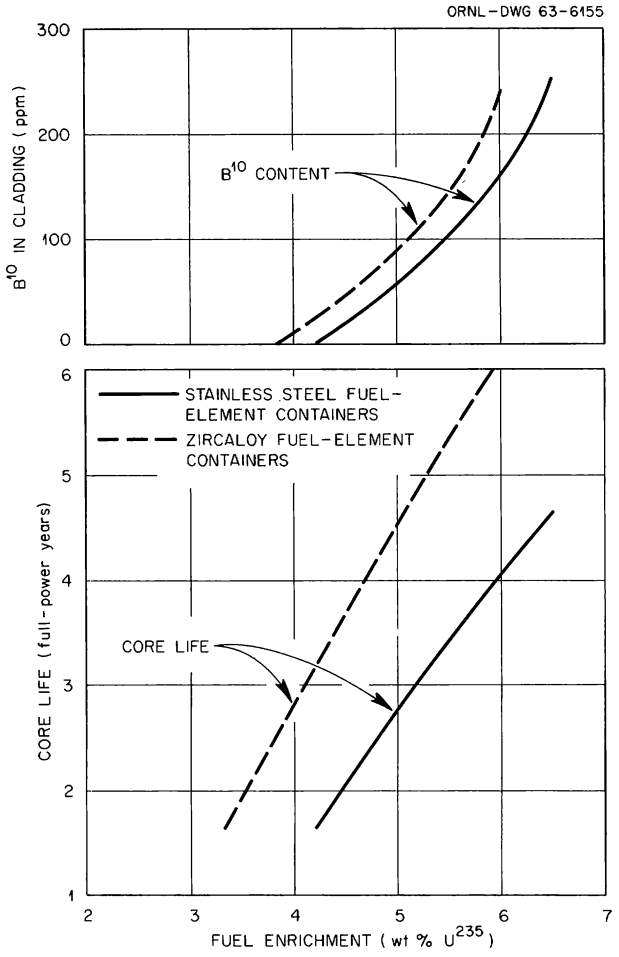

Fig. 3.2. Core Lifetime and Burnable Poison Content vs Fuel Enrichment for N.S. SAVANNAH-Type Cores Using Zircaloy and Stainless Steel Fuel-Element Containers.

Detailed Boron Burnable Poison Calculation

A more detailed burnup calculation of the longest lived core was made to determine the limitations of the simple burnup model. This calculation was made with the CANDLE code[5] using four groups of neutrons. Cross sections were obtained as described in ref. 1, except for the thermal group. The higher fuel loadings and the boron in the fuel cladding significantly

[5]O. J. Marlowe and P. A. Ombrellaro, CANDLE, A One Dimensional Few-Group Depletion Code for the IBM-704, USAEC Report WAPD-TM-53 and Addendum 1, Westinghouse Electric Corporation, October 1957.

"hardened" the thermal-neutron energy spectrum, so the method of calculating the thermal cross sections was modified as described in ref. 3.

Detailed burnup calculations were made for a core with Zircaloy fuel-element containers, fuel containing an initial loading of 6 wt % ^{235}U, and initial ^{10}B loadings of both 200 and 300 ppm in the stainless steel cladding of the fuel elements. The multiplication factors obtained as a function of time in these detailed calculations are compared in Fig. 3.3 (dashed curves) with the multiplication factors calculated with the use of Eq. (1) (solid curves). It is evident that Eq. (1) force fitted to a detailed calculation for fuel containing 4.2 wt % ^{235}U overestimates the initial core reactivity when extrapolated to a 6 wt % ^{235}U loading. While Eq. (1) and the detailed calculation agree on the worth of ^{10}B (i.e., 100 ppm of ^{10}B decreases core reactivity by 0.05 Δk), Eq. (1) overestimates the peak rise in reactivity as ^{10}B is consumed.

Additional calculations were made with the method described in ref. 1 to estimate the worth of the control rods. It was found that, relative to the Zircaloy fuel-element container core with 4.2 wt % ^{235}U and no boron poison, the control rods were worth less by the amount 0.02 Δk. Thus to be able to shut down the heavily loaded reactor at any point in life,

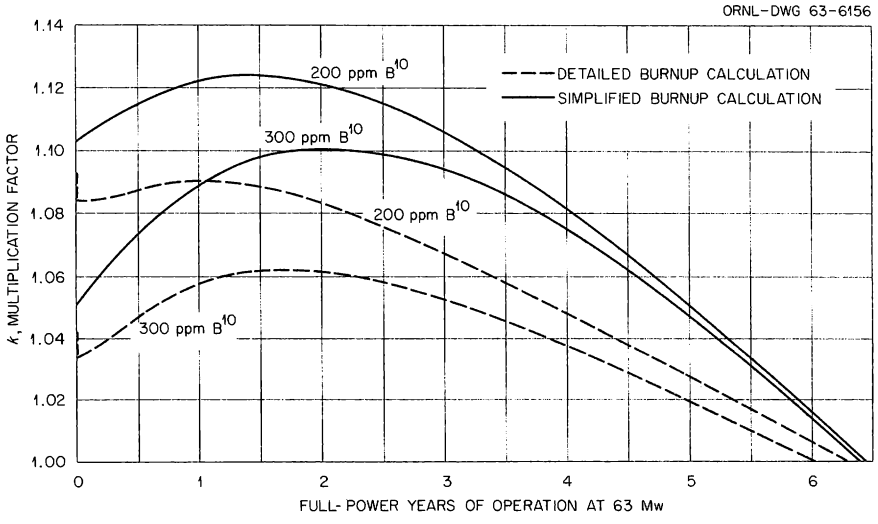

Fig. 3.3. Comparison of Results of Simplified Burnup Calculation with Those of Detailed Burnup Calculation for the N.S. SAVANNAH-Type Core with 6 wt % ^{235}U-Enriched Fuel and Zircaloy Fuel-Element Containers.

the hot multiplication factor should not be allowed to exceed the value k = 1.09 rather than the value k = 1.11. To limit the hot multiplication factor to 1.09, the detailed burnup calculations would lead to an initial ^{10}B loading of about 250 ppm (see Fig. 3.3). This ^{10}B loading is somewhat less than the value obtained from the simple burnup analysis, which ignored the change in rod worth as a function of core loading. Despite the obvious limitations of Eq. (1), the predicted core life for the above initial core loadings is within about 5% of that obtained with a more detailed calculation. Thus the use of Eq. (1) for a parametric study of core life vs fuel loading over the range 3 to 6 wt % ^{235}U should be satisfactory to establish general trends in fuel cycle costs.

Fuel-Cycle Cost Analyses

The physics calculations served to define the salient features of the two families of N.S. SAVANNAH cores of Fig. 3.2. The two families are characterized by the material used in the fuel element containers; that is, Zircaloy or stainless steel. Within a family of cores the members are outwardly distinguishable by core lifetime expressed in full-power years (fpy).

Fuel-cycle cost analyses were made for the two families of cores, and the results are shown in Figs. 3.4 and 3.5 for cores with stainless steel and Zircaloy fuel-element containers, respectively. The assumptions and ground rules used in these cost analyses, including an assumed load factor of 0.67, were the same as those employed in previous N.S. SAVANNAH fuel-cycle cost studies,[6,7] with the exception of uranium prices. Previous analyses were based on 1961 uranium prices, whereas the present results are based on the lower 1962 uranium prices. Since working capital cost is a component not always included in fuel-cycle cost analyses, the

---

[6]C. L. Whitmarsh, Potential Fuel-Cycle Cost Savings Resulting from Technological Changes in the N.S. SAVANNAH Reactor, USAEC Report ORNL-TM-144, Oak Ridge National Laboratory, April 6, 1962.

[7]T. D. Anderson et al., Summary Report — An Evaluation of the Substitution of Zircaloy for Stainless Steel in N.S. SAVANNAH Fuel Element Containers, USAEC Report ORNL-3476, Oak Ridge National Laboratory, Oct. 23, 1963.

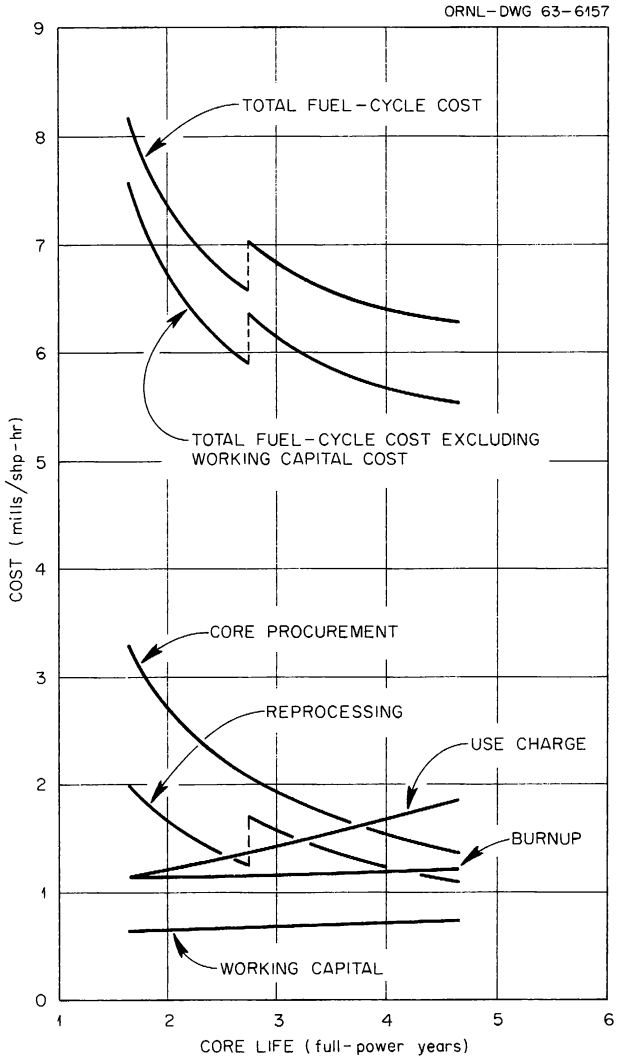

Fig. 3.4. Effect of Core Life on Fuel-Cycle Cost for N.S. SAVANNAH-Type Core with Stainless Steel Fuel-Element Containers.

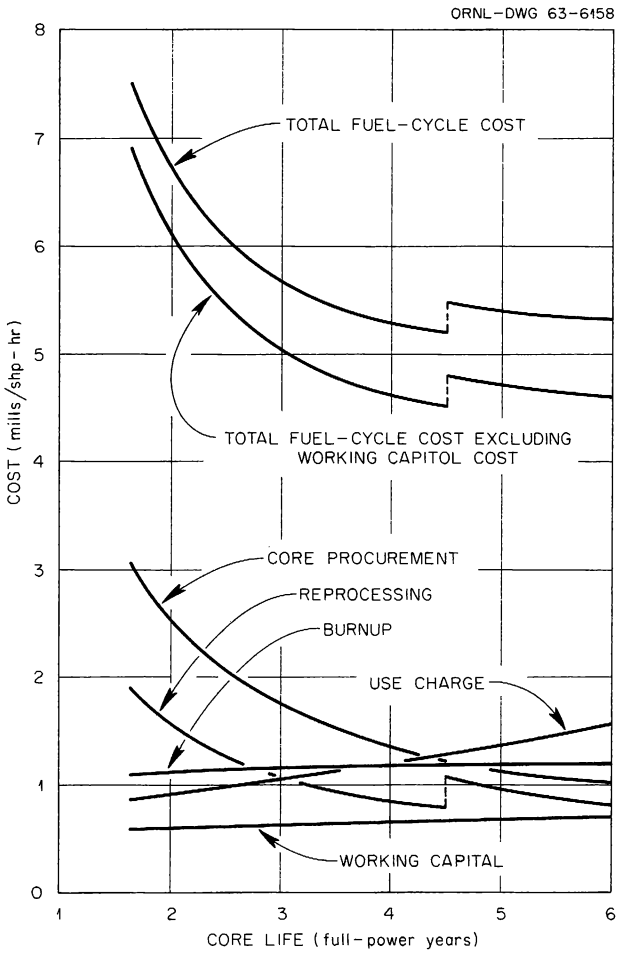

Fig. 3.5. Effect of Core Life on Fuel-Cycle Cost for N.S. SAVANNAH-Type Core with Zircaloy Fuel-Element Containers.

total fuel-cycle costs in Figs. 3.4 and 3.5 are given both with and without the cost of working capital. Costs associated with reactor refueling are excluded from the results.

The discontinuity in reprocessing cost, which occurs at an enrichment of 5 wt % ^{235}U, arises from the charges for converting UNH to UF_6. For enrichments of 5% and less the conversion cost is $5.60 per kg of uranium, and for enrichments greater than 5% the cost is $32.00 per kg.[8]

To give a cost comparison of Zircaloy and stainless steel fuel-element containers, the total fuel-cycle costs of Figs. 3.4 and 3.5 are replotted in Fig. 3.6. The costs shown in Fig. 3.6 are expressed as a fraction of core I fuel-cycle costs. As would be expected, the Zircaloy costs fall considerably below those of stainless steel.

The existence of the discontinuity in the fuel-cycle cost creates some uncertainty concerning the incentive for increasing core life to greater than 2.75 fpy for the stainless steel case and 4.5 fpy for the

---

[8]Guide to Nuclear Power Costs Evaluation, Vol. I, Reference Data and Standards, USAEC Report TID-7025, Sec. 110, p. 15ff, March 15, 1962.

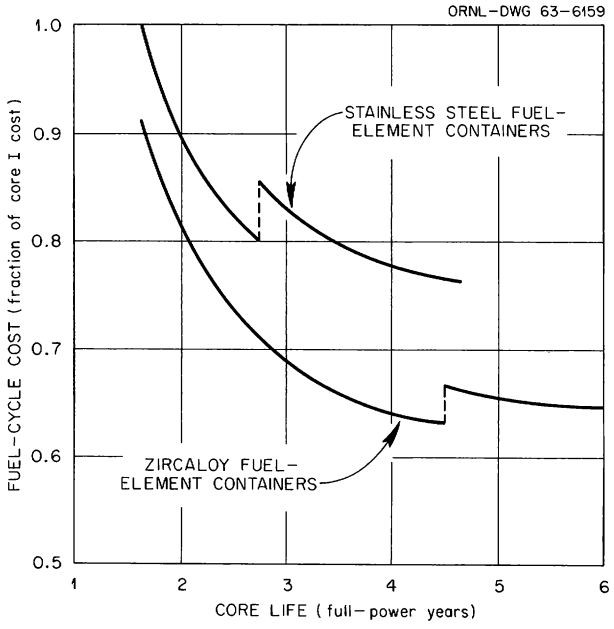

Fig. 3.6. Comparison of Fuel-Cycle Costs for N.S. SAVANNAH-Type Core with Zircaloy and Stainless Steel Fuel-Element Containers.

Zircaloy case. When the cost of refueling is considered[3] there appears to be an incentive to increase the stainless steel core life beyond the 2.75-fpy discontinuity to about 4.5 fpy. There seems to be no advantage in increasing the life of the Zircaloy core beyond 4.5 fpy.

Problems Associated with Long-Lived Cores

It has been shown in the preceding sections that by increasing the fuel enrichment and by adding ^{10}B to the fuel cladding, cores with ample reactivity life time can be built and that fuel cycle costs can be reduced. The cost reduction hinges on the condition that corrosion or failure due to high ^{10}B or fuel burnup or some other condition does not shorten the life of the core. No detailed investigation of these problems was made, but a cursory survey of the important problem areas was conducted to give an indication of the magnitude of the metallurgical problems.

A recent survey by Rabin[9] of the status of technology of austenitic stainless steels containing small amounts of boron revealed the following information:

1. Boronated steels containing up to 600 ppm boron are readily fabricated into tubing.

2. The quality of welds produced using stainless steels with up to 300 ppm boron equals that for normal stainless steels.

3. Fuel capsules with stainless steel cladding containing 300 ppm boron have been irradiated to boron burnups of about 2.4×10^{19} atoms/cm^3. Experimental evidence at higher boron burnups and the boron concentrations of interest here is nonexistent.

In high-flux regions of the core, essentially all the ^{10}B will be burned during the core lifetime. With 250 ppm of ^{10}B initially in the cladding, and assuming that all of it is burned, the boron burnup is about 12×10^{19} atoms/cm^3, or a factor of 5 greater than present experience, as outlined in item 3 above.

---

[9]S. A. Rabin, Status of Technology of Austenitic Stainless Steel Containing up to 0.1% Boron, Unpublished report, Oak Ridge National Laboratory, March 21, 1962.

For the 4.5-fpy cores the average UO_2 burnup would be about 14,000 Mwd/MT of UO_2. The maximum UO_2 burnup cannot be determined without detailed two dimensional burnup calculations, but the assumption that the peak-to-average burnup is the same as the peak-to-average power density gives an upper limit on burnup. With this assumption the maximum fuel burnup for the 4.5-fpy cores would be about 52,500 Mwd/MT of UO_2.

Several high-burnup irradiations were performed by General Electric[10] on plutonium-uranium oxide fuel pins containing both swaged and pelletized fuels. The fuels were solid solution of 20% plutonium oxide and 80% uranium oxide. The fuel pins were 0.190 in. in outside diameter and clad with stainless steel of 0.020-in. wall thickness. Of 40 fuel specimens, 10 were exposed to burnups exceeding 40,000 Mwd/MT of oxide, with the maximum exposure being 96,000 Mwd/MT. Maximum cladding surface temperatures during irradiations were 700 to 1200°F. None of the 40 specimens failed, and apparently no excessive swelling was observed.

Although very high UO_2-burnup data are limited, it is likely that with a proven cladding material, such as ordinary type 304 stainless steel, the N.S. SAVANNAH core could withstand a burnup corresponding to 4.5 fpy. Because of the interaction between the UO_2 and the cladding, these two fuel-element components cannot be considered separately. In view of the meager information on boronated cladding, it appears that high-burnup tests on prototype fuel elements would be useful in assessing their stability for 4.5 fpy.

UO_2 Fuel-Element Melting Calculations

T. D. Anderson

Correlation of UO_2 Fuel-Element Melting Data

An estimation of the power level at which fuel melting will occur is important to the design and safety evaluation of UO_2-fueled power reactors.

---

[10] J. M. Gerhart et al., The Irradiation and Examination of a Plutonium-Uranium Oxide Fast Reactor Fuel, ASTM Symposium on Radiation Effects in Refractory Fuel Compounds, ASTM Spec. Tech. Pub. No. 306, June 1961.

Likewise, accurate predictions of the amount of melting that will occur under prescribed irradiation conditions are fundamental to the study of melting-associated phenomena, such as fission-product release and fuel-element distortion. To provide the requisite fuel-to-cladding thermal conductance and thermal conductivity integral data for such calculations, an analysis was made[11] of Canadian data[12] for a group of 55 specimens irradiated in a hydraulic-rabbit facility. In conjunction with the Canadian irradiation results, the out-of-pile thermal conductivity measurements of Deem and Lucks[13] were used. These out-of-pile data were adjusted to account for irradiation effects[14] below about 1000°F.

The results of the analysis are shown in Figs. 3.7 and 3.8. Figure 3.7 gives the value of the integral $\int_{T_m}^{T_m} K(\theta)\, d\theta$ for UO_2 of 100% theoretical density, where T_m is the melting temperature of UO_2, $k(\theta)$ is the thermal conductivity of UO_2, and T is any UO_2 temperature (normally the UO_2 surface temperature, T_s). Figure 3.8 shows the fuel-to-cladding thermal conductance as a function of diametral clearance for elements filled with both helium and argon gases. Inferences (based on uninstrumented fuel-element experiments) concerning the interface conductance and the conductivity integral are always interrelated because it is never possible to obtain one without making assumptions about the other. Thus, the two sets of data given in Figs. 3.7 and 3.8 should be considered as an entity and should be used together.

The correlated data were used to calculate the measurable integral, $\int_{T_s}^{T_m} k(\theta)\, d\theta$, for the 55 specimens used in the correlation, and the calculated values agreed with the measured values within ±5.0% for 91% of the specimens, with the largest error being +7.0%. The correlation was

---

[11]Truman D. Anderson, Correlation of UO_2 Fuel-Element Melting Data, Trans. Am. Nucl. Soc., 6(2): 347 (November 1963).

[12]A. S. Bain et al., UO_2 Irradiations of Short Duration — Part II, Canadian Report CRFD-955, February 1961.

[13]H. W. Deem and C. F. Lucks, Thermal Conductivity of Uranium and UO_2, in Progress Relating to Civilian Application During January 1959, USAEC Report BMI-1315, pp. 7–9, Battelle Memorial Institute, Feb. 1, 1959.

[14]W. E. Roake, Irradiation Alteration of Uranium Dioxide, USAEC Report HW-73072, Hanford Atomic Products Operation, March 1962.

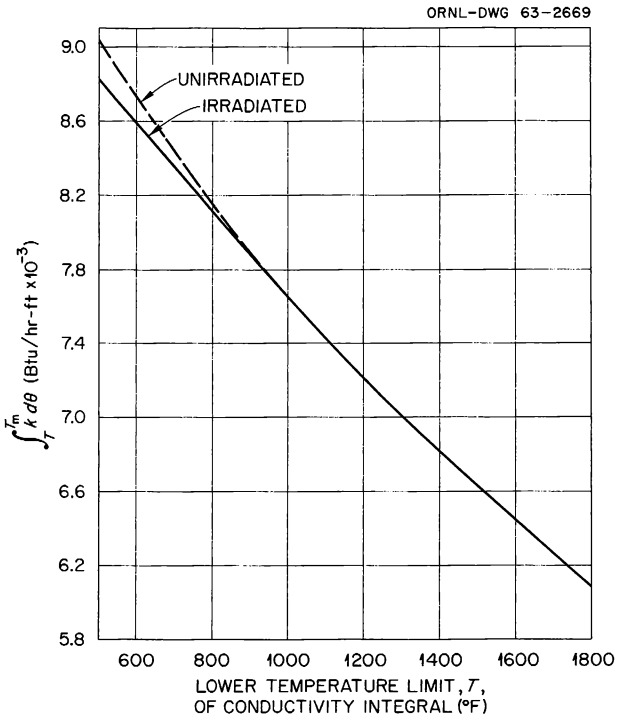

Fig. 3.7. UO_2 Thermal Conductivity Integral for Fuel-Element Melting Calculations (for 100% Theoretical Density Fuel).

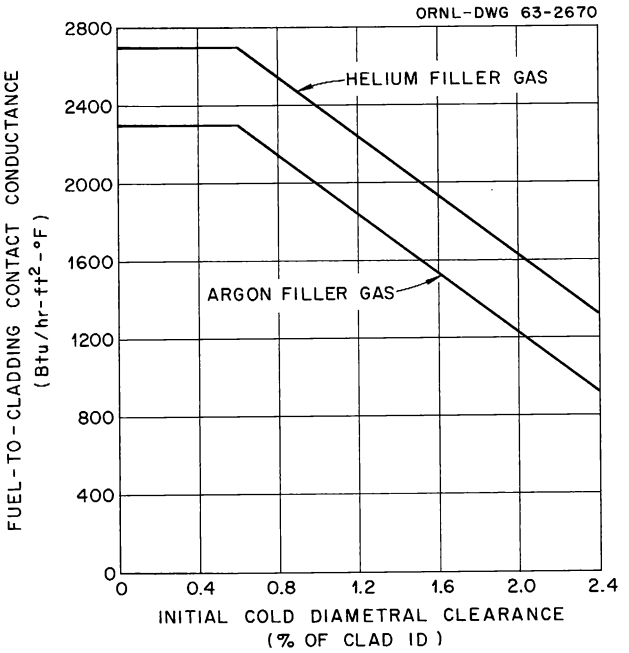

Fig. 3.8. Thermal Contact Conductance Between UO_2 and Cladding for Fuel-Element Melting Calculations.

also tested against data for eight specimens irradiated in a loop under conditions similar to those for water-cooled power reactors. The predictions agreed with the measurements within ±5.0% for six of the specimens, and the largest error was −10.0%. A summary of the comparisons of predicted with measured values is given in Fig. 3.9 for both the hydraulic-rabbit and loop specimens.

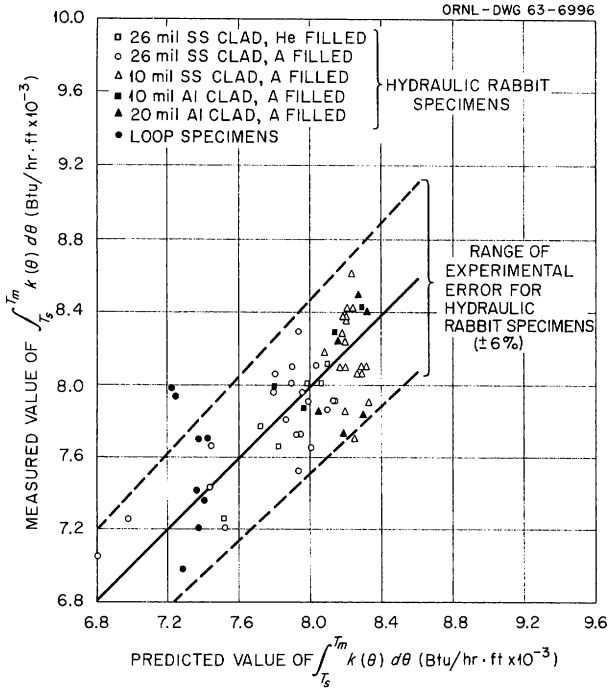

Fig. 3.9. Comparison of Measured and Predicted Values of $\int_{T_s}^{T_m} k(\theta)\,d\theta$ for Hydraulic Rabbit and Loop Fuel-Element Specimens.

Comparison of Calculated Fuel-Melting Conditions for Several Fuel Elements

The information in Figs. 3.7 and 3.8 was used to determine the linear power outputs at which fuel melting would occur in six water-cooled power reactors. The results are presented in Table 3.3. All the reactors considered have either been built or are under construction and were selected to give a representative cross section of current reactors of the water-cooled bulk-UO_2-fueled low-enrichment type. The reactor characteristics

Table 3.3. Power Outputs Necessary for Fuel Melting

Reactor with Initial Core	Estimated Fuel-Rod Linear Power Output for Fuel Melting (kw/ft)	Reactor Power for Fuel Melting (% of normal power)	
		Present Estimate[a]	Designers' Estimate
Big Rock Point	25.2	241	(b)
CVTR	22.6	161	(b)
Humboldt Bay	26.6	256	150
MH-1A	27.0	171	142
N.S. SAVANNAH	25.5	244	160
Yankee	23.6	203	(b)

[a]Based on assumption that core power distribution does not change with power level.

[b]Not available from hazards summary report.

used in the analyses were obtained from hazards summary reports[15-19] and are listed in Table 3.4. No attempt was made in the analyses to obtain conservative results; rather, the objective was to obtain realistic results for all systems on a consistent basis. As may be seen in Table 3.3, the estimated fuel-rod linear power outputs required for fuel melting do not vary much from reactor to reactor and, in general, range from 23 to 27 kw/ft. It is probable that this range of heat ratings for fuel melting

[15]Carolinas-Virginia Nuclear Power Associates, Inc., Final Hazards Summary Report, Part B, License Application, Report CVNA-90 (Pt. B, Vol. IV), Jan. 12, 1962.

[16]The Martin-Marietta Corp., Initial Hazards Summary Report for the MH-1A Floating Nuclear Power Plant, Vol. I, Engineering and Construction, May 1962.

[17]Pacific Gas & Electric Co. Technical Specifications, Humboldt Bay Power Plant, Unit No. 3, Docket 50-133, Amendment No. 12, Oct. 16, 1961.

[18]Yankee Nuclear Power Station Technical Information and Final Hazards Report, Vol. I, Part B, License Application, Docket 50-29, Sept. 15, 1959.

[19]Final Hazards Summary Report for Big Rock Point Plant, Vol. I, Plant Technical Description and Safeguard Evaluation, Docket 50-155, Nov. 14, 1961.

Table 3.4. Core Data Used in Fuel-Melting Analyses[a]

Reactor With Initial Core	Cladding				Fuel		Fuel-to-Cladding Initial Cold Diametral Gap (in.)	Fuel-Rod Peak Linear Heat Output at Normal Reactor Power (kw/ft)
	Material	Outside Diameter (in.)	Wall Thickness (in.)	Outer Surface Temperature[b] (°F)	Density (% of theoretical)	Enrichment[c] (% ^{235}U)		
Big Rock Point	Type 304 stainless steel	0.388	0.019	551	94[d]	3.2	0.005	10.5
CVTR	Zircaloy-4	0.4875	0.023	596	93	1.5	0.0115	14.0
Humboldt Bay	Type 304 stainless steel	0.463	0.019	547	95	2.6	0.005	10.4
MH-1A	Type 304 stainless steel	0.507	0.023	605	94	4.9	0.0045	15.8
N.S. SAVANNAH	Type 304 stainless steel	0.500	0.035	617	93	4.2	0.0045	10.4
Yankee	Type 348 stainless steel	0.340	0.021	636	92	3.4	0.004	11.6

[a] All dimensions are nominal values.

[b] Outer wall temperature assumed to be the saturation temperature at design pressure.

[c] Where there was more than one enrichment zone, the value for the innermost zone was used in the analysis.

[d] Assumed.

is typical of the general class of reactors characterized by the six that were considered.

Also shown in Table 3.3 are the reactor power levels (expressed as percentage of normal power) that would be required to cause fuel melting. Each of the reactor powers necessary for melting was obtained by dividing the linear power output for fuel melting by the peak linear power output at the normal reactor power. Where available, the designers' estimates of reactor powers required for fuel melting are shown for comparison with the present estimates.

Fuel Irradiation Tests

V. O. Haynes W. C. Thurber
E. L. Long, Jr.

A series of experiments involving the irradiation of nonpelletized UO_2 fuel were conducted in the ORR pressurized-water loop. The purpose of these tests was to determine the suitability of such fuel for use in a replacement core for the N.S. SAVANNAH, and thus the specimens were 0.5-in.-OD rods consisting of UO_2 clad with type 304 stainless steel of 0.035-in.-wall thickness. The fabrication techniques used were described in previous reports.[20-24].

---

[20]R. J. Beaver, J. T. Lamartine, and W. C. Thurber, Rotary Swaging of Stainless Steel-Clad UO_2 Fuel Rods, pp. 50–52, Maritime Reactor Project Ann. Progr. Rept. Nov. 30, 1960, USAEC Report ORNL-3046, Oak Ridge National Laboratory.

[21]J. T. Lamartine, Fuel-Rod Swaging Studies, pp. 79–80, Maritime Reactor Program Ann. Progr. Rept. Nov. 30, 1961, USAEC Report ORNL-3238, Oak Ridge National Laboratory.

[22]W. S. Ernst, Jr., Fabrication Studies on Vibratory Compaction of Fuel, pp. 89–92, Maritime Reactor Program Ann. Progr. Rept. Nov. 30, 1961, USAEC Report ORNL-3238, Oak Ridge National Laboratory.

[23]W. S. Ernst, Jr., and J. W. Tackett, Preparation of Irradiation Test Specimens for ORR Loop, pp. 75–77, Maritime Reactor Program Ann. Progr. Rept. Nov. 30, 1962, USAEC Report ORNL-3416, Oak Ridge National Laboratory.

[24]W. S. Ernst, Jr., Vibratory-Compaction Development, pp. 83–86, Maritime Reactor Program Ann. Progr. Rept. Nov. 30, 1962, USAEC Report ORNL-3416, Oak Ridge National Laboratory.

Irradiation Conditions

Twenty-seven nonpelletized fuel rods were irradiated in clusters of three in the pressurized-water loop, with high-purity water at 1750 psi and about 500°F flowing past the specimens at a rate of approximately 10 fps. Typical irradiation specimens are shown in Fig. 3.10, which is a preirradiation photograph of the specimen assemblies for experiment 7. Eighteen of the specimens (experiments 1, 3, 4, and 6) were examined destructively at the General Electric Company's Vallecitos Atomic Laboratory. The other nine specimens (experiments 5, 7, and 8) were examined at ORNL. The general characteristics of the specimens are summarized in Table 3.5.

Table 3.5. Description of Nonsintered UO_2 Fuel Specimens Irradiated in the ORR Pressurized-Water Loop

Experiment No.	Specimen No.	UO_2 Specimen Characteristics[a]					Fabrication Method	Fueled Length of Rod (in.)
		^{235}U Content (wt %)	Particle Size (mesh)	Density (% of theoretical)[b]	Surface Area (m^2/g)	Oxygen-to-Uranium Ratio		
1	1A1	2.03	−20 +35	90	0.27	2.027	Cold swaged	16 3/8
	1B1	2.03	−20 +35	90	0.27	2.026	Cold swaged	16 3/8
	1C1	2.04	−170 +325	87	0.46	2.017	Cold swaged	16 3/8
	1N1	0.80	−170 +325	89		2.021	Cold swaged	16 3/8
	1O1	0.83	−20	90	0.17	2.026	Hot swaged	16 3/8
	1P1	0.83	−20	90	0.14	2.024	Hot swaged	16 3/8
3	3A1	2.03	−20 +35	90	0.27	2.019	Cold swaged	16 3/8
	3B1	2.03	−20 +35	90	0.33	2.025	Cold swaged	16 3/8
	3C1	2.04	−170 +325	87	0.41	2.021	Cold swaged	16 3/8
	3N1	0.80	−170 +325	89	0.36		Cold swaged	16 3/8
	3O1	0.83	−20	90	0.18	2.030	Hot swaged	16 3/8
	3P1	0.83	−20	90	0.19	2.024	Hot swaged	16 3/8
4	4N1	1.87	−20 +35	90.5	0.03	<2.001	Cold swaged	16 1/4
	4O1	1.87	(c)	87.2	0.05	<2.001	Vibration compacted	16 1/4
	4P1	1.12	(c)	88.1	0.08	2.002	Vibration compacted	16 1/4
5	5A1	3.78	(c)	88.2	0.07	2.002	Vibration compacted	16 1/4
	5B1	4.22	(c)	88.0	0.12	2.002	Vibration compacted	16 1/4
	5C1	4.22	−20 +35	91.0	0.02	<2.002	Cold swaged	16 1/4
6	6N1	2.85	(c)	88.0	0.07	2.004	Vibration compacted	16 1/4
	6O1	2.85	(c)	87.9	0.07	2.004	Vibration compacted	16 1/4
	6P1	2.85	(c)	87.5	0.07	2.004	Vibration compacted	16 1/4
7	7N1	5.09	(d)	87.1		2.002	Vibration compacted	16 1/4
	7O1	5.09	(d)	87.1		2.002	Vibration compacted	16 1/4
	7P1	5.09	(d)	86.9		2.002	Vibration compacted	16 1/4
8	8N1	5.09	(e)	85.8	0.13	2.003	Vibration compacted	16 1/4
	8O1	5.09	(e)	85.8	0.13	2.003	Vibration compacted	16 1/4
	8P1	5.09	(e)	85.5	0.13	2.003	Vibration compacted	16 1/4

[a] All specimens contained fused and ground UO_2 prepared by Spencer Chemical Co., except the specimens for experiment 8, which contained sintered and crushed UO_2.

[b] Theoretical density taken to be 10.97 g/cm^3.

[c] 60 ± 1 wt % −10 +16 mesh, 15 ± 1 wt % −70 +100 mesh, 25 ± 1 wt % −200 mesh.

[d] 62.2 wt % −10 +16 mesh, 16 wt % −70 +100 mesh, 21.8 wt % −200 mesh.

[e] 60 wt % −4 +16 mesh, 15 wt % −70 +100 mesh, 25% −200 mesh.

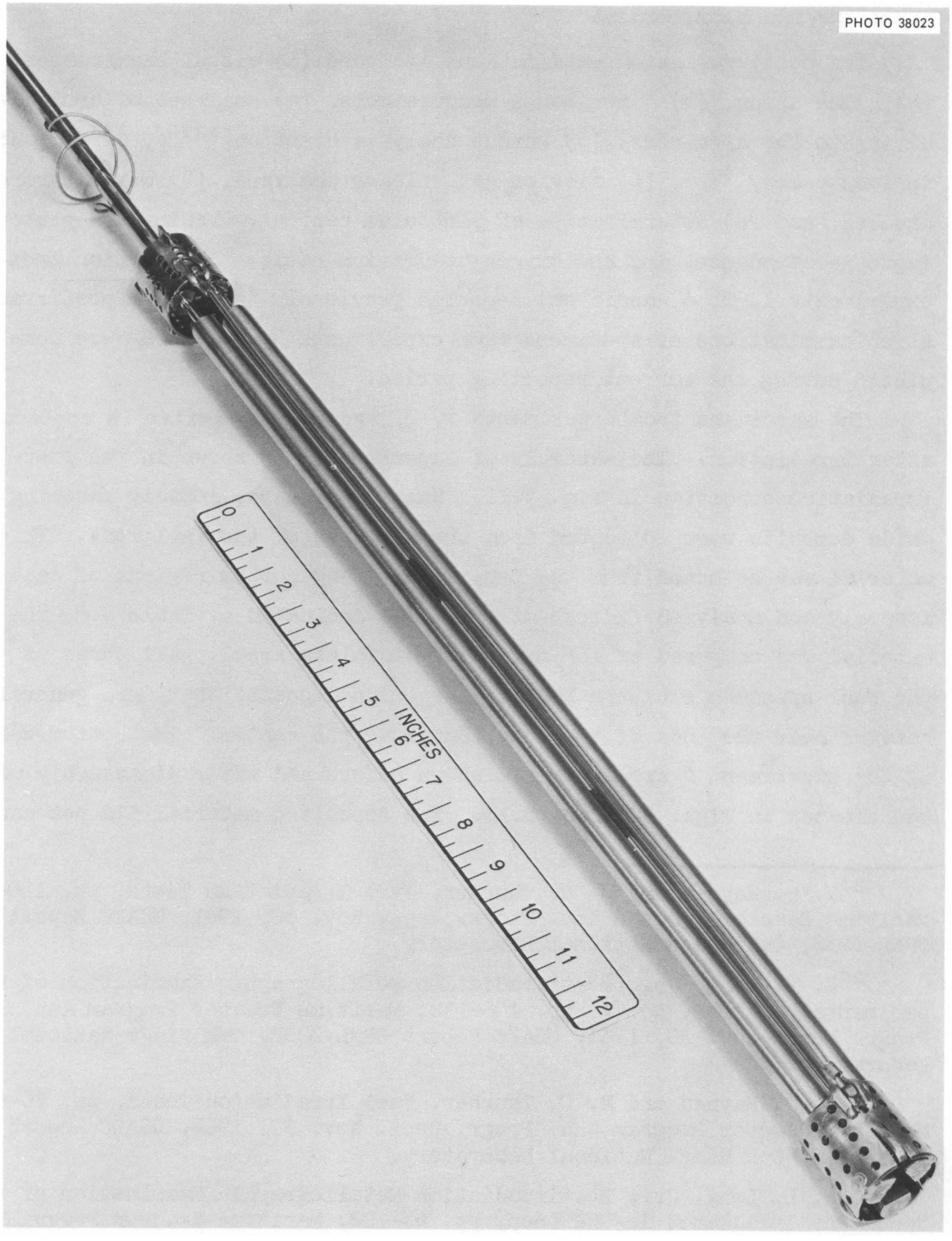

Fig. 3.10. Irradiation Test Assembly for Experiment 7 Prior to Irradiation.

Postirradiation Examination

The postirradiation examinations included (1) visual examination, (2) gamma scans, (3) dimensional measurements, (4) analyses of crud adhering to the specimens, (5) burnup analysis based on ^{137}Cs, ^{144}Ce, and, in some cases, ^{95}Zr, (6) fission-gas-release analyses, (7) metallographic studies, and (8) determination of plutonium content, uranium and plutonium isotopic abundance, and the oxygen-to-uranium ratio. Information from experiments 1, 3, 4, and 6 was reported previously.[25-28] The postirradiation examinations of specimens from experiments 5, 7, and 8 were completed during the current reporting period.

The specimens from experiments 5, 7, and 8 were similar in appearance after irradiation. The assembly of experiment 5 is shown in the postirradiation condition in Fig. 3.11. Samples of dark, loosely adhering oxide deposits were collected from the surfaces of the fuel rods. This material was selected from the top, middle, and bottom regions of each assembly and analyzed radiochemically. As indicated by Table 3.6, the material was composed of the oxides of stainless steel. All three of the fuel specimen clusters had similar oxide deposits that were generally heavier near the ends of the rods than near the center. The bottom ends of the experiment 5 specimens are shown before and after disassembly of the cluster in Figs. 3.12 and 3.13. The deposited material did not cause

---

[25]V. O. Haynes and W. C. Thurber, Fuel Irradiation Tests, pp. 100–105, Maritime Reactor Program Ann. Progr. Rept. Nov. 30, 1961, USAEC Report ORNL-3238, Oak Ridge National Laboratory.

[26]E. L. Long, Jr., Postirradiation Metallographic Examination of Experimental Assembly No. 1, pp. 106–112, Maritime Reactor Program Ann. Progr. Rept. Nov. 30, 1961, USAEC Report ORNL-3238, Oak Ridge National Laboratory.

[27]V. O. Haynes and W. C. Thurber, Fuel Irradiation Tests, pp. 86–95, Maritime Reactor Program Ann. Progr. Rept. Nov. 30, 1962, USAEC Report ORNL-3416, Oak Ridge National Laboratory.

[28]E. L. Long, Jr., Postirradiation Metallographic Examination of Fuel Specimens Irradiated in ORR Loop, pp. 95–102, Maritime Reactor Program Ann. Progr. Rept. Nov. 30, 1962, USAEC Report ORNL-3416, Oak Ridge National Laboratory.

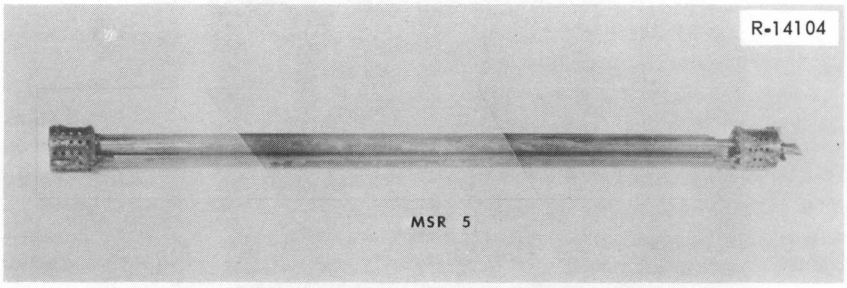

Fig. 3.11. Irradiation Test Assembly for Experiment 5 After Irradiation.

Table 3.6. Results of Radiochemical and Chemical Analyses of Samples of Crud from Experiment 5, 7, and 8 Specimens

	Experiment 5 Specimens		Experiment 7 Specimens		Experiment 8 Specimens		
	Top	Bottom	Top	Bottom	Top	Middle	Bottom
Sample weight, mg	44	155	55	116	164	494	627
Average crud concentration on specimen surface, mg/cm^2	1.1	7.6	3.6	7.6	1.5	4.6	5.9
Nuclide concentration of crud, dps/g ($\times 10^{-6}$)							
^{55}Fe (2.94y)	73	79.6	117	153	134	252	144
^{59}Fe (45.1d)	79	97.2	141	177	141	284	186
^{58}Co (72.0d)	104	174	125	288	301	678	414
^{60}Co (5.27y)	44.8	54.8	52.9	76.8	71.9	170	115
^{54}Mn (300d)	13.2	22.9	14.2	36.0	22.6	41.5	28.1
^{51}Cr (27.8d)	232	181	<170	443	379	163	377
Element concentration of crud, g/g							
Fe	0.33	0.356	0.316	0.327	0.352	0.586	0.394
Co	<0.006	<0.002	<0.005	<0.002	<0.004	<0.002	<0.003
Mn	(a)	(a)	(a)	<0.0005	0.001	0.0014	0.0011
Cr	0.001	0.002	0.002	0.002	0.0014	0.0014	0.0018
Ni	0.079	0.093	0.100	0.104	0.048	0.069	0.056
Al	0.023	0.009	0.022	0.011	(b)	(b)	(b)
Mo	(a)	0.002	(a)	0.002	(b)	(b)	(b)
Zr	0.004	0.002	0.003	0.002	0.002	0.0013	0.0055

[a] Not detected.

[b] Not determined.

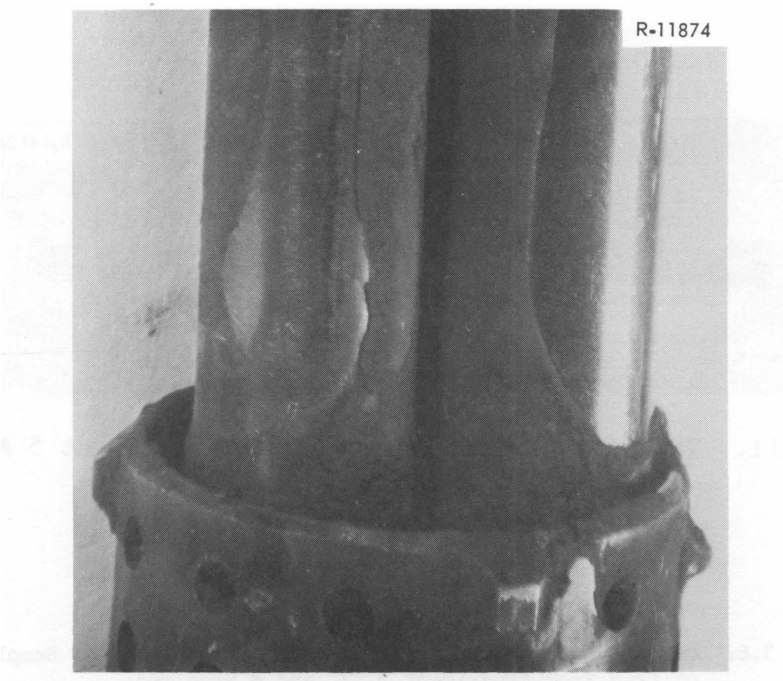

Fig. 3.12. Lower End of Experiment 5 Specimens Following Irradiation; Before Disassembly.

Fig. 3.13. Lower End of Experiment 5 Specimens Following Irradiation; After Disassembly.

failures of any of the rods, but it undoubtedly increased the temperatures experienced by the specimen and probably considerably changed the temperature distribution, especially in the cladding, from that which prevailed initially without the crud deposits. No other irradiation effects were detected by the visual examination.

The gamma scans were similar to those obtained from the previously examined specimens. A broad maximum in gamma intensity occurred about 6 in. from the bottom of each rod, as illustrated by Fig. 3.14, which is the gamma scan of rod P of experiment 7. A slight amount of flux peaking was indicated at the ends of most rods. Peak-to-average values for the gamma scans were about 1.15, which is about the same as observed for the previously examined specimens. The fuel rods that operated at temperatures sufficiently high to produce central voids exhibited more irregular gamma scans than the lower performance fuel rods. These irregularities are probably associated with fission-product migration and

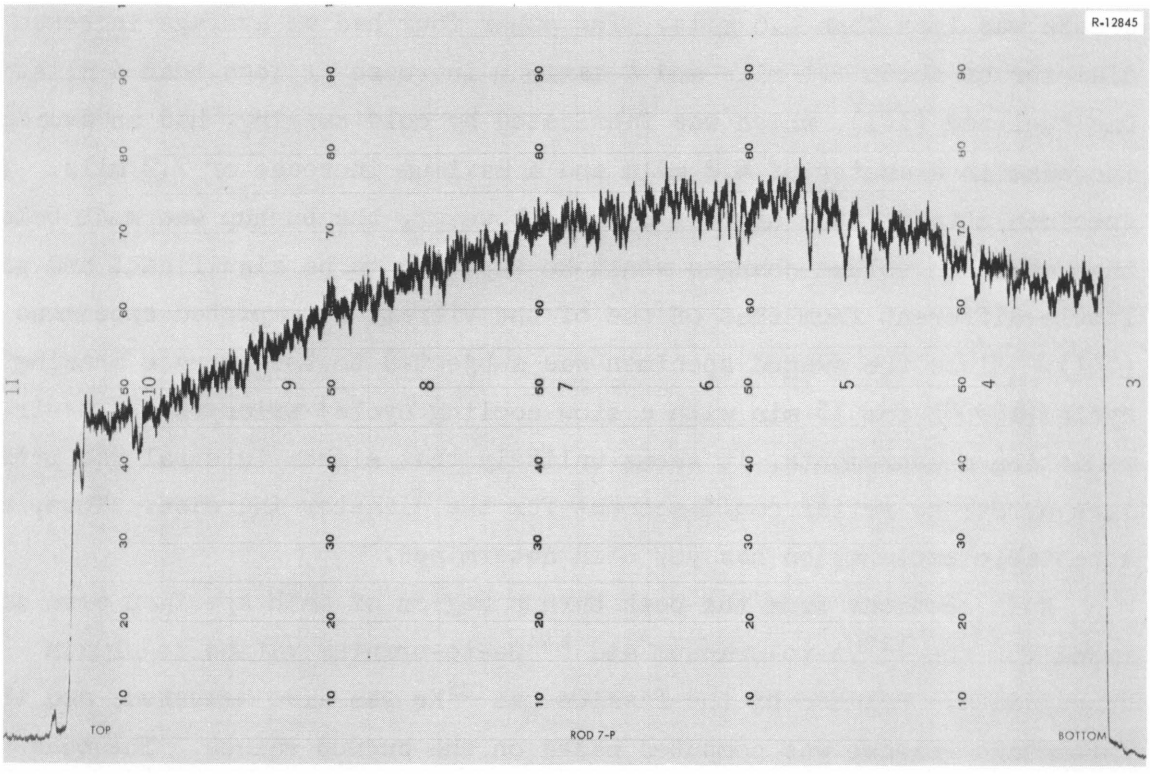

Fig. 3.14. Gamma Scan of Fuel Specimen 7P1.

possibly with fuel segregation or movement. Subsequent analysis of fuel sectioned from the peak flux region indicated migration of ^{137}Cs in fuel rods having central voids. This is apparent from the burnup data tabulated later in this section.

Dimensional examination of the assemblies included inter-rod spacing and bow measurements. Rod diameters were measured after cluster disassembly. Preirradiation measurement techniques were duplicated as nearly as possible in the postirradiation examination.

Rod profiles from the bow measurements of seven of the nine rods indicated a change in the outward direction; one indicated an inward bow; and one was essentially unchanged. Broken rod-to-spacer braze joints probably contributed to the bowing of rod B of experiment 5 and rod P of experiment 8. Rod P of experiment 8 exhibited by far the most bow — a change of approximately 0.050 in. between pre- and postirradiation measurements.

Of the eight rods fabricated by vibratory compaction, four had an average increase in diameter of about 0.5 mils; the maximum diameter increase was less than 1.6 mils. The other four had an average increase in diameter of about 1.5 mils and a maximum increase of less than 4 mils. One fuel rod (5CI), which was fabricated by cold swaging, had an average increase in diameter of 4.2 mils and a maximum increase of 7.7 mils. This specimen attained the highest burnup; however, the burnup was much below that at which volume changes would be expected to be significant and was little different from that of one of the vibration compacted specimens (5B1). Since the swaged specimen was subjected to the furnace brazing cycle (1850°F for 15 min with a slow cooling cycle) prior to the preirradiation measurements, it seems unlikely that either internal gas pressure or stress relief could account for the diameter increase. Thus, no acceptable explanation has yet been determined.

Fuel sections from the peak burnup region of each specimen were analyzed for the ^{137}Cs-to-uranium and ^{144}Ce-to-uranium ratios to obtain burnup data. Release of the fission gas ^{85}Kr was also measured, and the percentage release was computed based on the burnup values. The peak burnup and ^{85}Kr release are given in Table 3.7 for all 27 specimens.

Table 3.7. Burnup and Fission-Gas-Release Data

Experiment No.	Specimen No.	Peak Heat Rating (w/cm)	Peak Burnup[a] (Mwd/MT of U)	^{85}Kr Release[b] (%)	Kr Release[c] (%)
1	1A1	110	940	0.72	
	1B1	135	1120	4.98	
	1C1	140	1280	6.05	
	1N1	130	1040	6.02	
	101	130	1070	2.53	
	1P1	160	1300	3.44	
3	3A1	105	2480	3.7	
	3B1	125	3030	3.4	
	3C1	130	3320	7.6	
	3N1	130	2950	3.3	
	301	130	2900	3.1	
	3P1	160	3820	3.2	
4	4N1	285	3120	4.12	
	401	250	2870	2.19	
	4P1	220	2440	2.93	
6	6N1	305	3750	4.74	
	601[d]	340	4150	10.51	
	6P1[d]	375	4660	23.43	
5	5A1	160	6530	2.3	1.6
	5B1	185	7760	7.6	2.4
	5C1	200	8250	4.3	2.3
7	7N1	390	4720	12.4	7.5
	701	415	5070	47	11
	7P1	505	6210	72	15
8	8N1	370	4750	77	19
	801	385	4970	25	15
	8P1	515	6790	25	33

[a]Based on fission product ^{144}Ce analysis and 205 Mev per fission.

[b]Calculated with reference to burnup based on ^{144}Ce.

[c]Calculated from mass spectrometric analysis with reference to burnup based on ^{144}Ce.

[d]Data for specimens 601 and 6P1 are given in exchanged order from that reported by GE-VAL; the order given here is believed to be correct.

Changes from values reported previously reflect refinement of or corrections to the previous information.

Isotopic abundance and oxygen-to-uranium ratios were not determined for experiments 5, 7, and 8. The experiment 8 specimens were analyzed for ^{239}Pu content, and the peak concentrations were found to be 0.48, 0.37, and 1.36 mg of ^{239}Pu per gram of uranium, respectively.

Metallography of Irradiated Fuel

Transverse sections were taken from each of the fuel rods from experiments 5, 7, and 8 at the regions of maximum burnup for metallographic examination, as shown in Fig. 3.15. An additional metallographic specimen was taken from rod "N" of experiment 7 at the end of the central void and prepared for a transverse examination. Three of the lower spacers that had been brazed to the fuel rods were also examined metallographically.

Specimens from Experiment 5. The specimen that was taken from rod 5C1 was the only one from experiment 5 that showed any evidence of microstructural changes as a result of irradiation. Sintering had occurred to a radial distance of 0.110 in. from the center of the fuel column. Representative areas from the outer surface and central regions of this fuel rod are shown in Fig. 3.16.

Although a lamellar precipitate had formed in the inner surface regions of the cladding in fuel rod 5B1 to a maximum depth of 3 mils, as

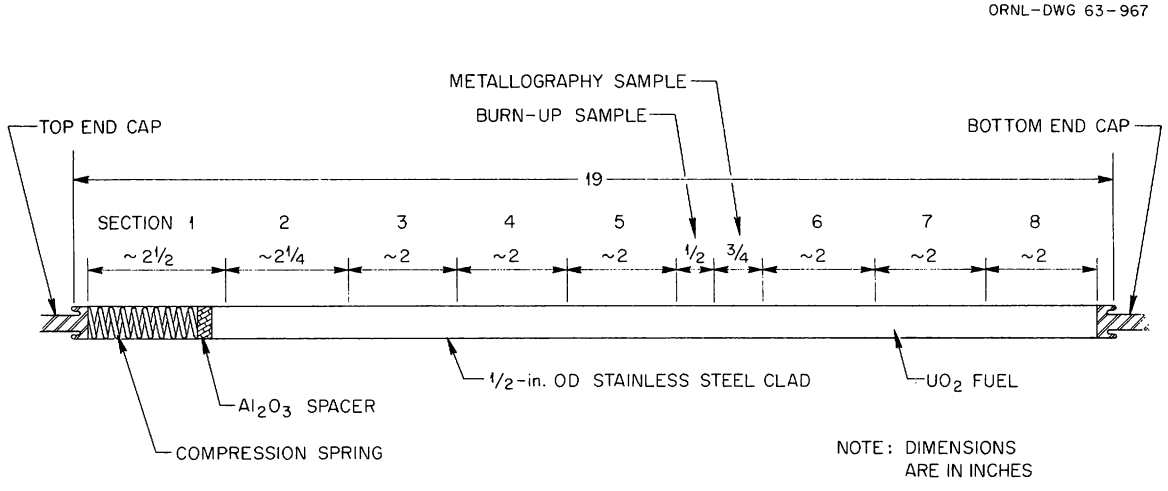

Fig. 3.15. Diagram for Sectioning Irradiated Fuel Rods.

PHOTO 68271

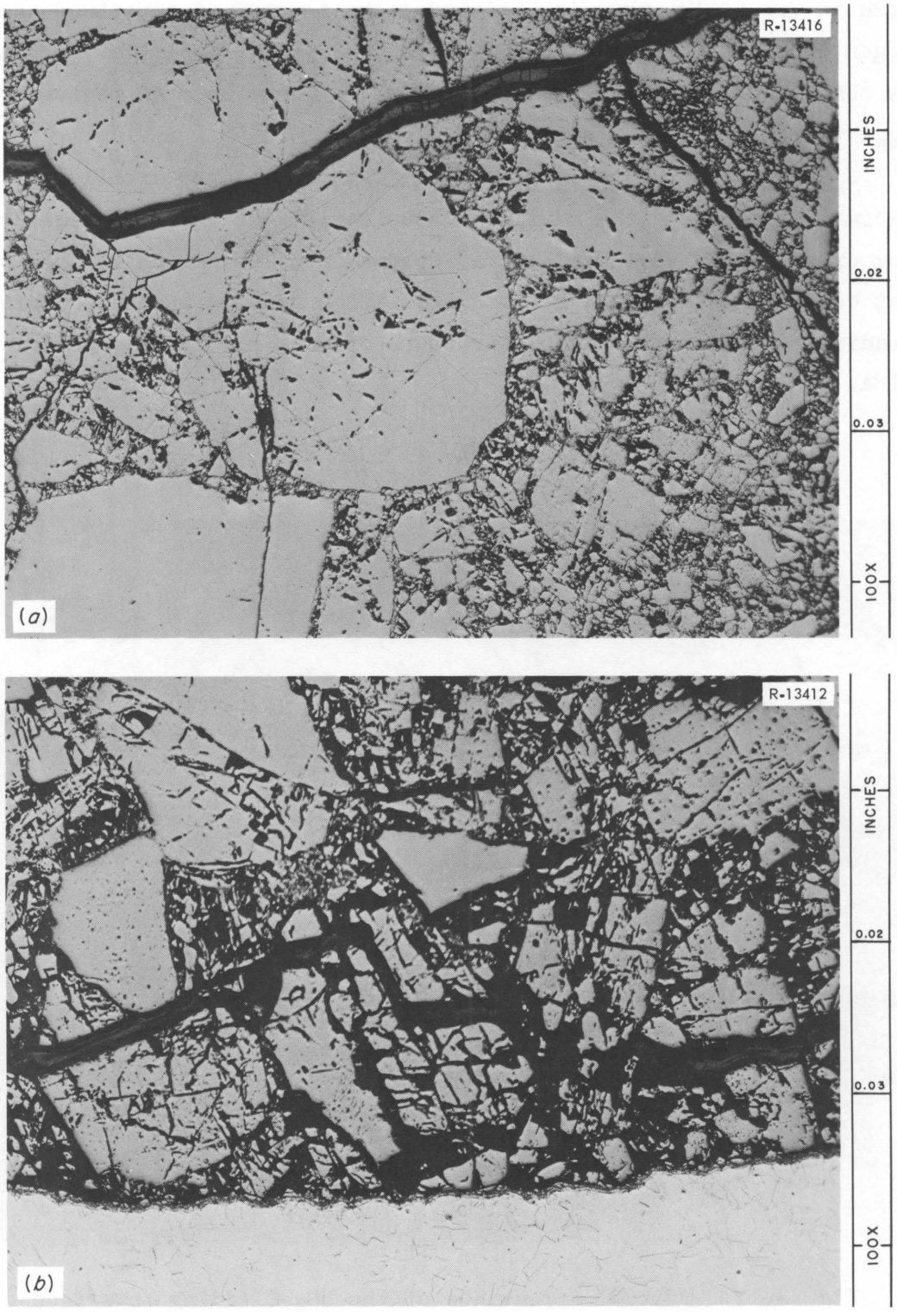

Fig. 3.16. Representative Areas from the (a) Central Region and (b) the Cladding-Fuel Interface of Fuel Rod 5C1. Etched. 100X (Original reduced 10%)

shown in Fig. 3.17, this is believed to be a combined effect of the nitrogen content of the fuel and the brazing cycle. A similar phenomenon was observed in previous experiments.[26,28] There were no regions that suggested potential failure of the cladding.

Specimens from Experiment 7. The microstructural details of the specimens taken from the maximum burnup regions of the three fuel rods from experiment 7 were similar in appearance. The extent of the changes that occurred as a result of the irradiation test is shown in Table 3.8. A radial panorama of the microstructure of fuel rod 7N1 is shown in Fig. 3.18a.

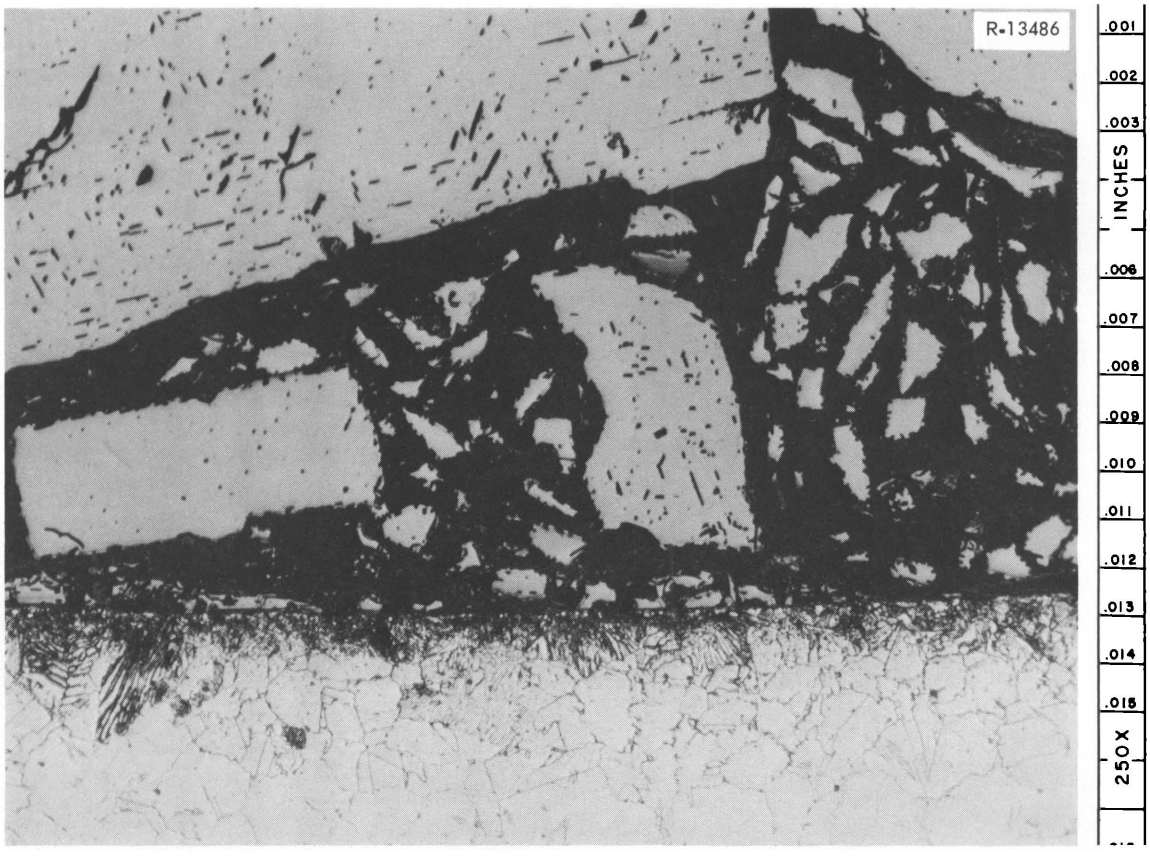

Fig. 3.17. Typical Appearance of the UO_2-Cladding Interface of Fuel Rod 5B1. The lamellar precipitate visible in the cladding to a depth of approximately 3 mils is believed to be a nitride that formed during fabrication. Etched. 250X

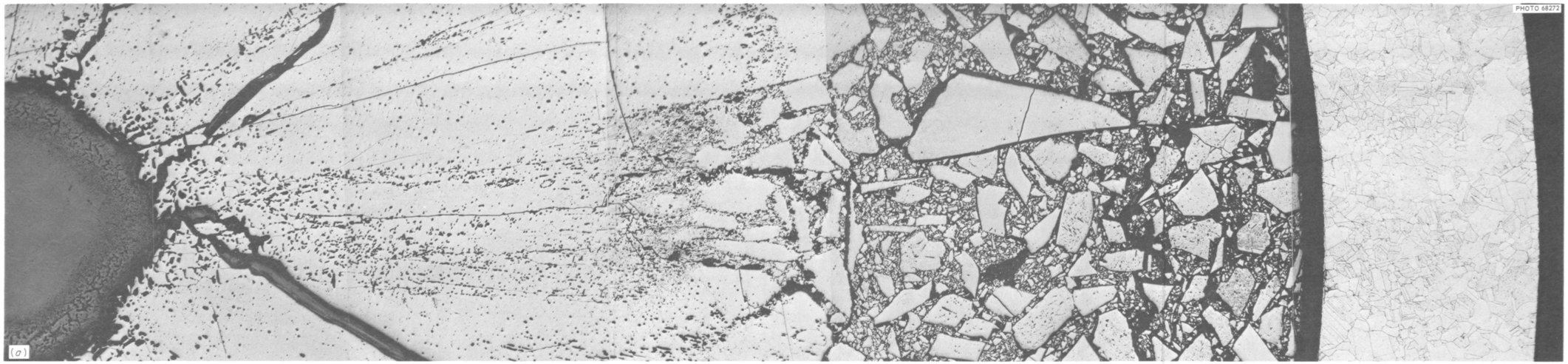

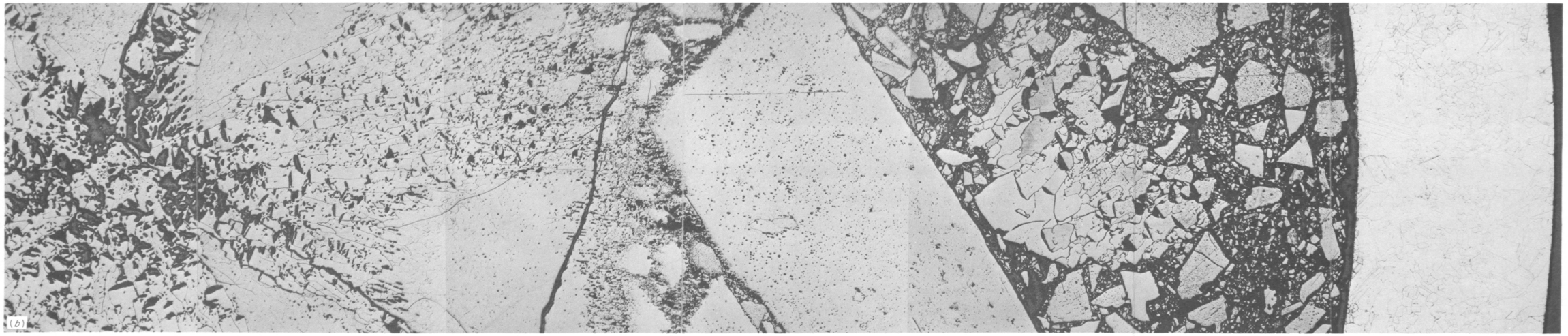

Fig. 3.18. Radial Panoramas Made from Transverse Sections Through Fuel Rod 7N1. This fuel rod contained fused and crushed UO_2. (a) From a specimen taken at the point of maximum burnup. (b) From a specimen taken at the end of the central void in the fuel column. Note the presence of lenticular voids between the large particle of UO_2 and the cladding. Etched. 100X (Original reduced 32%)

Table 3.8. Radial Extent of Microstructural Changes Observed in Specimens from Experiment 7

Fuel Rod	Central Void (in.)	Columnar Grain Growth (in.)	Sintering (in.)
7N1	0.025	0.135	0.180
701	0.025	0.140	0.195
7P1	0.032	0.160	0.175

In addition to the metallographic specimen taken from the point of maximum burnup, another specimen was taken at the end of the central void in the fuel column. A radial panorama of this specimen is shown in Fig. 3.18b. The unusual feature observed in this specimen was that a localized hot-spot existed in the fuel at approximately 0.025 in. from the type 304 stainless steel cladding, as can be seen in the figure. The presence of lenticular voids in the fuel in this localized region indicated a temperature excursion to at least 1600°C some time during the irradiation test.[29] In spite of the localized hot-spot, the cladding showed no evidence of potential failure in any of the specimens examined from experiment 7.

Specimens from Experiment 8. As it was with the specimens from experiment 7, those taken from experiment 8 at regions of maximum burnup were similar in appearance. However, a difference was noted between the specimens taken from the two experiments. A radial panorama showing the microstructural details of the specimen taken from fuel rod 8N1 is shown in Fig. 3.19. As can be seen, a region of equiaxed grain growth existed at the end of the columnar grain growth. There was no evidence of equiaxed grain growth in any of the specimens taken from experiment 7. The extent of the changes that occurred as a result of the irradiation test is shown in Table 3.9. The microstructure of the type 304 stainless steel cladding appeared to be normal.

[29] V. B. Lawson and J. R. MacEwan, Thermal Simulation Experiments with a UO_2 Fuel Rod Assembly, Canadian Report CRFD-915, March 1960.

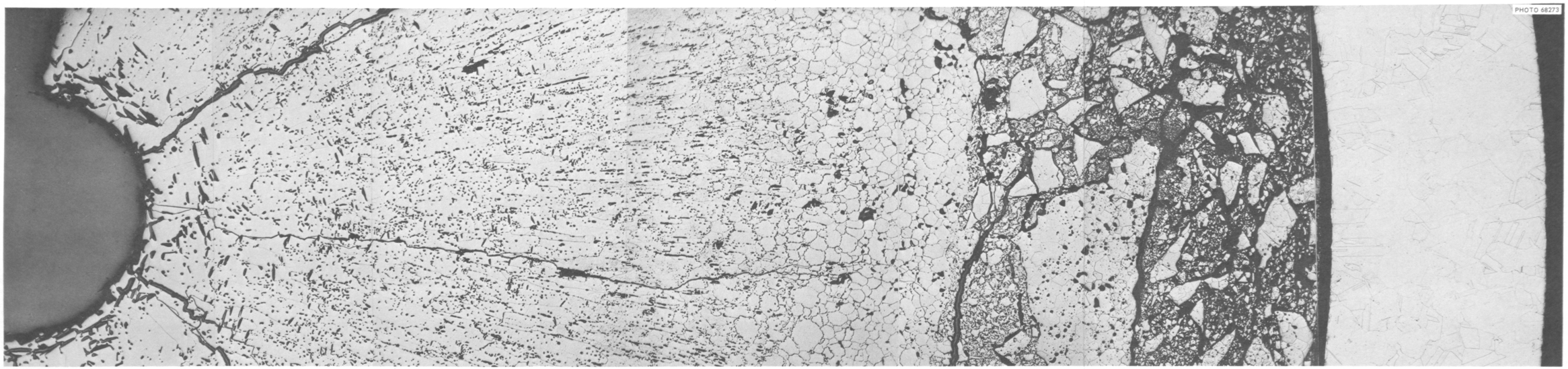

Fig. 3.19. A Radial Panorama Taken from a Transverse Section Through Fuel Rod 8N1 at the Region of Maximum Burnup. Etched. 100X (Original reduced 21%)

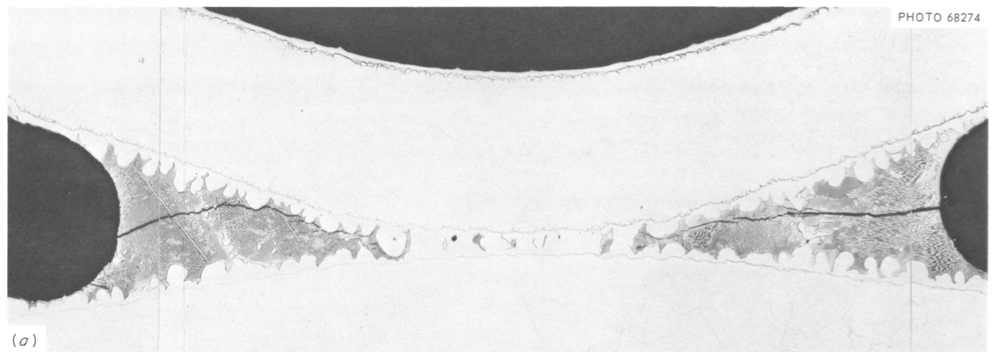

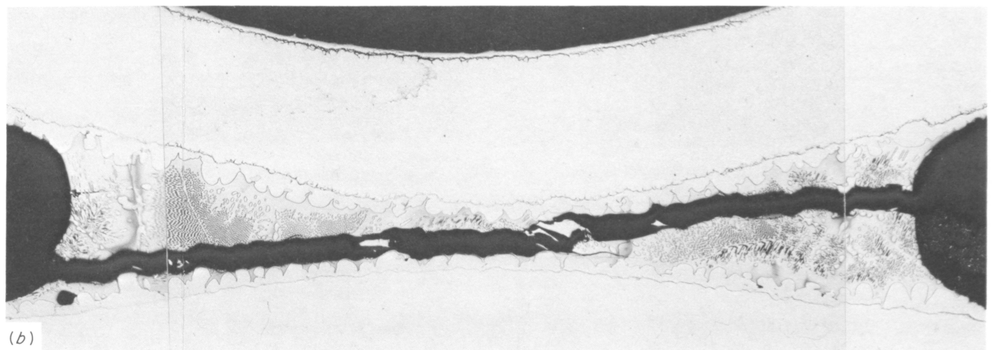

Fig. 3.20. Ferrule-to-Cladding Electroless-Nickel-Brazed Joints. (a) Joint that remained intact throughout the irradiation test; from fuel rod 801. (b) Failed joint from fuel rod 8P1. Joint failed as a result of the formation of a continuous brittle phase. Electrolytically etched. 100X

Table 3.9. Radial Extent of Microstructural Changes Observed in Specimens from Experiment 8

Fuel Rod	Central Void (in.)	Columnar Grain Growth (in.)	Equiaxed Grain Growth (in.)	Sintering (in.)
8N1	0.020	0.115	0.145	0.150
801	0.028	0.130	0.155	0.160
8P1	0.038	0.148	0.160	0.200

Ferrule-to-Cladding Brazed Joints

Three ferrule-to-cladding electroless-nickel brazed joints were examined metallographically. One of the brazed joints examined was the bottom ferrule from the assembly of experiment 5 that fell apart during disassembly. The other two examined were the brazed joints of the bottom ferrule to fuel rods 8P1 and 801. Of these three joints, only one remained intact after the irradiation test. Apparently, the ferrules in the joints that failed were not in close enough contact with the cladding during the brazing cycle to prevent a continuous layer of the brittle eutectic from forming through the brazed joint. Only the joint that remained intact was similar in appearance to those rated as acceptable in the original investigations of electroless-nickel brazed joints for the Maritime fuel bundles.[30] The results of this examination are shown in Fig. 3.20.

[30]J. T. Lamartine and W. C. Thurber, Status Report — Application of Electroless Nickel Brazing to Tubular Fuel Elements for the N.S. SAVANNAH, USAEC Report ORNL-CF-59-6-55, Oak Ridge National Laboratory, June 2, 1959.

Previous reports in this series are:

ORNL-2656 Maritime Reactor Project Ann. Prog. Rep. Nov. 30, 1958
ORNL-2865 Maritime Reactor Project Ann. Prog. Rep. Nov. 30, 1959
ORNL-3046 Maritime Reactor Project Ann. Prog. Rep. Nov. 30, 1960
ORNL-3238 Maritime Reactor Program Ann. Prog. Rep. Nov. 30, 1961
ORNL-3416 Maritime Reactor Program Ann. Prog. Rep. Nov. 30, 1962

ORNL-3775

UC-80 – Reactor Technology
TID-4500 (37th ed.)

Internal Distribution

1. R. E. Adams
2. T. D. Anderson
3. V. E. Anderson (K-25)
4. C. F. Baes, Jr.
5. S. E. Beall
6. R. J. Beaver
7. E. P. Blizard
8. A. L. Boch
9. C. J. Borkowski
10. G. E. Boyd
11. R. B. Briggs
12. W. E. Browning, Jr.
13. F. R. Bruce
14. J. Buchanan
15. D. W. Cardwell
16. C. E. Center
17. F. L. Carlsen, Jr.
18. T. E. Cole
19. J. A. Conlin
20. W. B. Cottrell
21. J. A. Cox
22. F. L. Culler
23. J. E. Cunningham
24. I. T. Dudley
25. E. P. Epler
26. W. K. Ergen
27. W. S. Ernst, Jr.
28. B. R. Fish
29. A. P. Fraas
30. J. H. Frye, Jr.
31. R. G. Gilliland
32. J. C. Griess
33. W. R. Grimes
34. E. E. Gross
35. V. O. Haynes
36. M. R. Hill
37. D. O. Hobson
38. W. H. Jordan
39. S. I. Kaplan
40. G. W. Keilholtz
41. O. H. Klepper
42. J. A. Lane
43. C. E. Larson (K-25)
44. E. L. Long, Jr.
45. R. N. Lyon
46. H. G. MacPherson
47. E. R. Mann
48. H. C. McCurdy
49. H. F. McDuffie
50. A. J. Miller
51. E. C. Miller
52. K. Z. Morgan
53. F. H. Neill
54. M. L. Nelson
55. P. Patriarca
56. A. M. Perry
57. M. E. Ramsey
58. A. F. Rupp
59. H. W. Savage
60. A. W. Savolainen
61. J. L. Scott
62. O. Sisman
63. M. J. Skinner
64. G. M. Slaughter
65. A. H. Snell
66. I. Spiewak
67. J. A. Swartout
68. J. W. Tackett
69. W. C. Thurber
70. D. E. Tidwell
71. D. F. Toner
72. D. B. Trauger
73. G. M. Watson
74. A. M. Weinberg
75. G. D. Whitman
76. M. L. Winton
77-78. Central Research Library
79-80. ORNL-Y-12 Technical Library
Document Reference Section
81-106. Laboratory Records Dept.
107. Laboratory Records, ORNL RC

External Distribution

108. Ira Adler, New York Operations Office, AEC
109-110. Col. R. B. Burlin, Division of Reactor Development (Army Reactors), AEC, Washington
111. J. J. Catalano, New York Operations Office, AEC
112. Capt. G. W. Chase, Marine Design Division, U.S. Army Engineer District, Philadelphia, Pa.
113-117. T. C. Christian, AEC-MARAD Joint Group, Galveston, Texas
118. B. W. Colston, Atomics International, Canoga Park, Calif.
119-120. D. F. Cope, Reactor Division, AEC, ORO
121-130. D. L. Crook, Office of Research and Development (Maritime Reactors), Washington, D.C.
131. Capt. R. D. Farmer, Nuclear Power Field Office, Ft. Belvoir, Va.
132. M. J. Letich, American Bureau of Shipping, New York, N.Y.
133. Zel Levine, Martin Company, Nuclear Division, Baltimore, Md.
134-137. W. F. Long, Babcock & Wilcox Company, Atomic Energy Commission, Lynchburg, Va.
138. J. H. MacMillan, Babcock & Wilcox Company
139-140. D. C. McMillan, George G. Sharp, Inc., New York
141. R. W. MacNamee, Manager, Research Administration, UCC
142-144. R. O. Mehann, Todd Shipyard Corporation, Nuclear Division, Galveston, Texas
145. L. J. Misenheimer, Nuclear Power Field Office, Ft. Belvoir, Va.
146-147. J. F. O'Brien, Martin Company, Nuclear Division
148. J. E. Robb, Bechtel Corporation, San Francisco, Calif.
149-150. C. E. Thomas, Babcock & Wilcox Company, N.S. SAVANNAH Technical Staff, Galveston, Texas
151. W. C. Stamm, Ebasco Services, Inc., New York
152-153. Commandant (MMT), U.S. Coast Guard, Washington, D.C.
154. Research and Development Division, AEC, ORO
155-770. Given distribution as shown in TID-4500 (37th ed.) under Reactor Technology category (75 copies - CFSTI).